Materials Science and Engineering R 122 (2017) 1–28

Contents lists available at ScienceDirect

Materials Science and Engineering R

journal homepage: www.elsevier.com/locate/mser

Review

On deformation behavior of Fe-Mn based structural alloys

Piyas Chowdhury[a], Demircan Canadinc[b], Huseyin Sehitoglu[a,*]

[a] Department of Mechanical Science and Engineering, University of Illinois at Urbana-Champaign, 1206 W. Green St., Urbana, IL 61801, USA
[b] Department of Mechanical Engineering, Koç University, 34450 Istanbul, Turkey

ARTICLE INFO

Article history:
Received 7 June 2017
Accepted 8 September 2017
Available online xxx

Keywords:
Manganese steel
TWIP steel
High entropy steel
Shape memory alloy
Strain hardening

ABSTRACT

This article is a literature review of recent advances in novel Fe-Mn based alloys, drawing specific examples on Hadfield and TWIP steels, and high entropy and shape memory alloys. A critical discussion of these alloys merits a uniform treatment owing to their remarkable mechanical attributes, i.e. a substantial combination of strength and ductility. It is interesting to note that their microscopic deformation mechanism also shares commonality in terms of twinning-dominated straining in addition to slip-based plasticity. In the past two decades alone, a synergy of materials science and mechanics based studies has significantly helped uncover the microstructural origin, effects of alloying etc. therein. In this paper, we discourse elaborately on the reported microstructure-property correlations. By surveying these developments, we point out how the current knowledgebase can pave the way for strategizing future materials advancements as well as expanding applications.

Contents

1. Introduction . . . 2
 1.1. Hadfield steels (HS) . . . 2
 1.2. Twinning induced plasticity (TWIP) steels . . . 3
 1.3. Shape memory alloys (SMAs) . . . 3
 1.4. High entropy alloys (HEAs) . . . 3
2. Hadfield steel . . . 4
 2.1. Single crystal deformation characteristics . . . 4
 2.2. Effect of nitrogen alloying . . . 4
 2.3. Role of aluminum addition . . . 5
 2.4. On strain-rate sensitivity and other properties . . . 6
 2.5. Future promises: alloy design, TWIP steels and high entropy alloys, advanced modeling . . . 8
3. Twinning induced plasticity (TWIP) steel . . . 9
 3.1. Micro-deformation mechanisms governing the strain hardening in TWIP steels . . . 10
 3.2. Deformation of TWIP steels at high strain rates . . . 11
 3.3. Modeling efforts: crystal plasticity . . . 14
 3.4. Case study: incorporation of slip-twin interactions on the deformation response of TWIP steels into crystal plasticity . . . 14
 3.5. TWIP steels: the first step towards next-generation steels . . . 15
4. Fe-Mn based shape memory alloys (SMAs) . . . 15
 4.1. Case study: Fe-Mn-Si and Fe-Mn-Si-Cr-Ni alloys . . . 16
  4.1.1. Deformation responses . . . 16
  4.1.2. Slip- assisted fcc ↔ hcp phase transformation and other considerations . . . 17
 4.2. Case study: Fe-Mn-Ni-Al alloys . . . 18
  4.2.1. Thermomechanical properties and microstructure . . . 18
  4.2.2. Slip-assisted bcc ↔ fcc transformation . . . 18

* Corresponding author.
E-mail address: huseyin@illinois.edu (H. Sehitoglu).

http://dx.doi.org/10.1016/j.mser.2017.09.002
0927-796X/

5. Fe-Mn based high entropy alloys (HEA) . . . 19
5.1. Structure-property correlation in CoCrFeMnNi HEAs . . . 19
5.1.1. Engineering of microstructure properties . . . 19
5.1.2. Observed deformation behavior . . . 20
5.1.3. A rationale for constitutive responses . . . 21
5.2. Temperature-dependent deformation response . . . 21
5.3. Fracture properties . . . 22
5.4. Role of substitutional elements . . . 22
5.5. Future promises: predicting new multi-component solid solutions . . . 24
6. Latest modeling approaches: atomistics . . . 24
6.1. Ab-initio predictions on Fe-Mn based alloys . . . 24
6.2. Effect of N addition in pure Fe . . . 24
7. Concluding remarks . . . 25
Acknowledgements . . . 26
References . . . 26

1. Introduction

Fe-Mn based alloys constitute several important classes of engineering materials with remarkable mechanical characteristics, which make them attractive in numerous industrial applications today (Fig. 1). Hadfield steels, which exhibit an unusually high work hardening rate under loading, are still being used in heavy industrial applications, such as caterpillar tracks, railroads, mining equipment, and crusher jaws, where high strength and wear resistance are necessary [1,2]. Twinning-induced plasticity (TWIP) steels find their applications mostly in the automotive industry, for example as the chassis, due to an excellent blend of high strength and lightweight [3–5]. The utilization of Fe-Mn based shape memory alloys (SMAs) are being actively investigated as seismic dampers [6]. Lastly, although not yet actively employed in industrial settings, high entropy alloys (HEA) hold considerable promise in cryogenic applications (e.g. in space-bound vehicles with liquefied fuel) due to their superior toughening attributes [7–9] at low temperatures. Given the diversified applications and potential of this class of materials, considerable research has been conducted to establish their structure-property correlations. The strength and ductility of these four classes of materials are compared with other structural alloys in Fig. 2. In this paper, we present an overview of the current knowledge base.

1.1. Hadfield steels (HS)

Discovered in 1925 by Sir Robert Hadfield [10], Hadfield steels possess austenitic (fcc) lattice structure with high Mn content. The high strain hardening, for which these steels find widespread industrial usage, has been attributed to interaction of dislocation slip with carbon interstitial and twinning systems [11–16]. These alloys present themselves as interesting case studies due to their propensity for increased strengthening attributes. This is primarily a direct consequence of alloying, which leads to considerably low stacking fault energy, an attribute very conducive to twinning [15]. From research perspective, considerable amount of works are recorded in the literature on the single and polycrystalline deformation mechanism, effects of alloying with nitrogen, aluminum etc. [17–21].

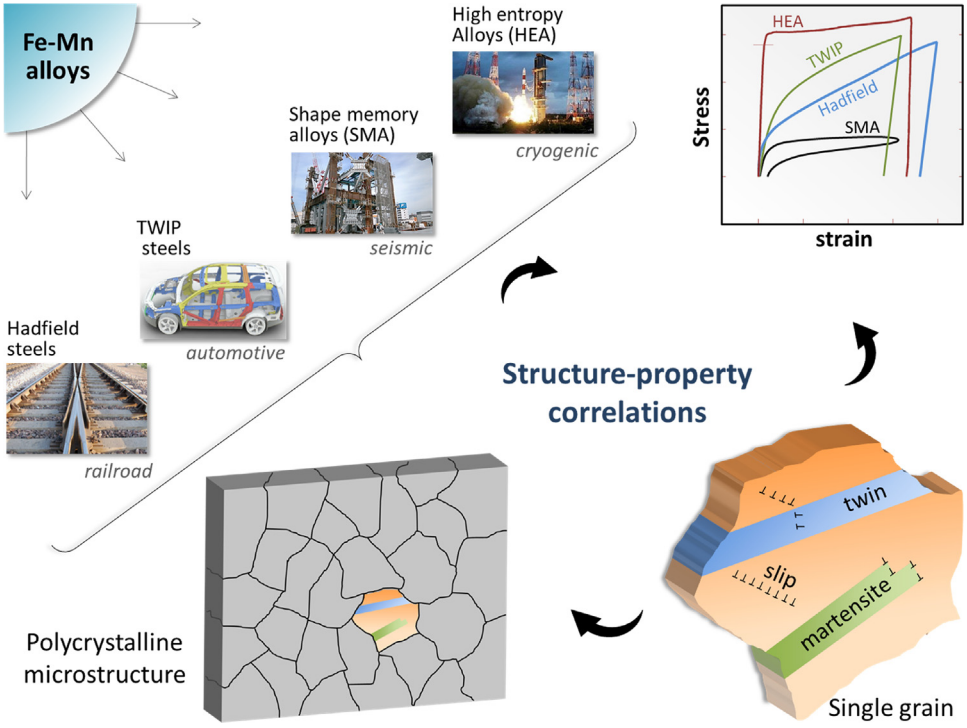

Fig. 1. Fe-Mn based alloys have diverse usage, both current and potential (e.g. in railroad, automotive, seismic and cryogenic applications). This paper reviews the reported structure-properties correlations in these materials.

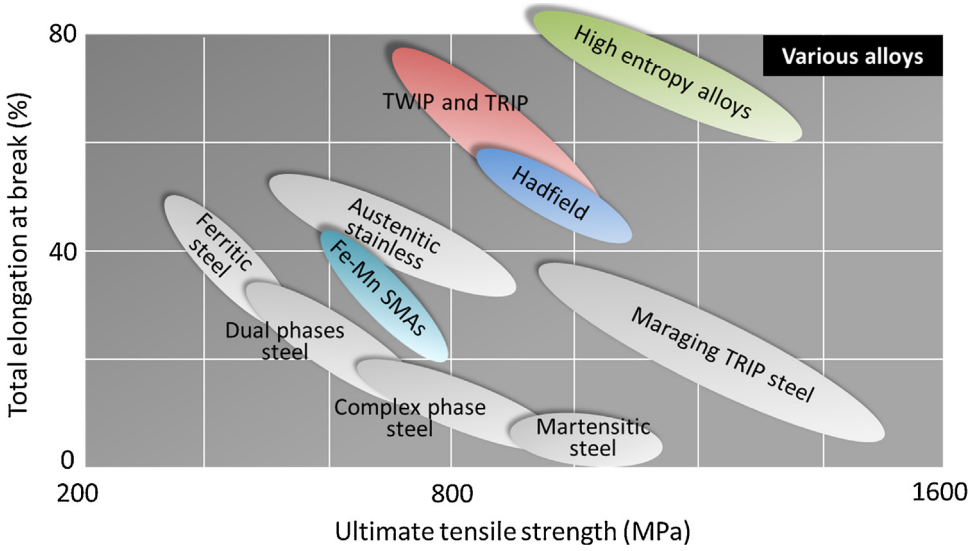

Fig. 2. Superior strength-ductility performance exhibited by TWIP and TRIP steels.

Specifically, extensive microstructure characterizations have been performed to establish a consistent picture of the deformation mechanism underlying the superior hardening effects in these materials [2,18–20,22,23]. For instance, the details of twin nucleation, formation of dislocation walls, interactions between these defects, as well as solute hardening and texture effects are examined. These revelations have benefitted significantly from modern characterization techniques, such as digital image correlation (DIC), electron microscopy, and electron backscatter diffraction (EBSD). In this paper, we discuss the key findings on the empirical mechanical behaviors of Hadfield single- and polycrystal materials along with the microstructure characterizations. A brief case study of constitutive modeling will also be presented to exemplify the ongoing research.

1.2. Twinning induced plasticity (TWIP) steels

TWIP steels are also austenitic steels having fcc crystal structure with a Mn content upwards of 20 wt% [24]. Similar to Hadfield steels, they possess low stacking fault energy (20–40 mJm^{-2}), which gives rise to prevalent twining-based mechanism during plastic deformation [25–27]. Consequently, a greater degree of slip obstruction is encountered due to a reduction of their mean free path for free gliding, which results in the superior flow strength [28–30]. Extensive studies have been directed at understanding, for example, the role of grain size/orientation, alloying, dislocation substructure evolution, promotion/suppression of twinning [3,4,31–39]. It was established that the gradual evolution of dislocation structure eventually leads to the deformation twinning at more advanced stages of deformation. Numerous studies confirmed these microscopic trends. In this paper, we cover the experimental hardening response of TWIP steels from representative works, and the associated microstructural changes revealed through techniques such as EBSD, electron microscopy.

1.3. Shape memory alloys (SMAs)

Shape memory alloys are known for their remarkable strain recovering ability by mere removal of load and/or by heating [40]. Fe-Mn based SMAs are particularly well-known due to the low costs of the constituent chemical species such as Fe, Mn, Si, Al, Cr. The main utility of Fe-Mn based SMAs alloys is related with engineering applications suitable near room temperature [41,42]. The microscopic deformation mechanism of strain recovery in these alloys is characterized by reversible fcc-to-hcp or bcc-to-fcc transformations [43–47] (fcc, bcc, hcp being face-centered cubic, body-centered cubic and hexagonal close-packed). Most SMAs (i.e. Ni-Ti and Cu based ones) have ordered lattice structure, and the shape recovery is dictated by two-way martensitic transformation. By contrast, the Fe-Mn SMAs are characterized by disordered lattice and a dislocation-assisted transformation mechanism. Since the microscopic mechanism is at the heart of the manifestation of global properties, a study of these materials in a single volume can provide important insight into how to further engineer the mechanistic characteristics to develop superior alloys. For instance, the mesoscopic factors that control the dislocation motion would also play a significant role in the shape recovering attributes such as the obstruction by grain boundaries, non-shearable precipitates and Cottrell atmosphere [48]. Drawing on specific case studies, we discuss the experimental constitutive characteristics of these alloys as well as their deformation mechanism(s).

1.4. High entropy alloys (HEAs)

Discovery of high entropy alloys is a very recent development [8,9,49–52]. What is unique of this class of alloys is that, unlike conventional alloys where elements are added to a base metal, HEAs are fabricated by mixing constituents in (nearly) equiatomic proportion. In this article, we cover the characteristics of equiatomic CoCrFeMnNi high entropy alloys (HEA), which have found recent interest due to their exceptional mechanical strength and ductility [8,53]. HEAs are single phase solid solutions with (near) equiatomic composition typically comprising five transition metals (or upwards) [7,9]. These alloys are characterized by high entropy of mixing, which in turn enhances solubility of individual chemical species. The properties of a HEA are typically considerably different from its constituent elements. Despite multiple types of solutes, each element has the same propensity to occupy a certain lattice site. Due to volumetric mismatch among different solute atoms from different constituent species, the lattice structure can be highly distorted [54]. The immediate effects of such distortion has been associated with high strengthening attributes [55,56]. In addition, due to a slow diffusion compared to conventional metals and alloys, the propensity of microscopic precipitate formation is rather high. One unique characteristic of

HEAs is that a dramatic change in mechanical properties can be achieved by tweaking the alloying contents [57–59].

From research standpoint, several outstanding issues are pinpointed. For instance, unlike binary or ternary alloys, no precise phase diagram has been uncovered to guide the design of multi-element HEA towards optimum properties. Another issue remains in the form of alloying-induced variation in the stacking fault energy, which in turn would largely control the mechanism of plastic deformation (e.g. slip-mediated versus twinning-dominated flow). A clear correlation between the composition and the fault energetics is necessary to accomplish desired plastic attributes. From current literature, the HEAs with bcc structure possess high strength with low ductility, while fcc HEAs have low strength with considerable elongation. This trend poses a possible strategy for the overall toughness improvement by mixing fcc and bcc types [60] by manipulating fabrication variables.

2. Hadfield steel

Hadfield steel, an austenitic manganese steel, is frequently used in mining and railroad frog applications, which require excessive deformation and wear resistance. Despite being discovered more than a hundred years ago, micro-deformation mechanisms of Hadfield steel, especially its unusually high work hardening capacity, are still being subject to scientific studies. Hadfield steel is mainly utilized in diverse applications, such as crawler treads for tractors, railroad frogs, grinding mill liners, crusher jaws and cones, impact hammers, dipper bucket teeth, and nonmagnetic plates for electromagnets [61]. The material possesses high toughness combined with ductility and high work hardening capacity, and excellent wear resistance.

The ASTM Standard [62] covering this steel allows composition ranges of 1.0–1.4 wt.% carbon, and 10.0–14.0 wt.% manganese. However, there are many variations in the original chemical composition of austenitic manganese steel. The compositional variations usually involve changes in carbon and manganese with or without additional alloys such as chromium, nickel, molybdenum, and titanium. The variation of carbon content in the Hadfield composition range does not provide a significant change in elongation. However, tensile strength and ductility increase with increasing manganese content despite the fact that increase in manganese content within the 10.0–14.0 wt.% range does not result in an increase in yield strength [61].

In general, Hadfield manganese steel castings are not useful in the as-cast form since the inevitable carbide formation leads to a loss of ductility and impact toughness, and possibly pearlite formation. The usual practice to produce high quality Hadfield steel is the heat treatment by austenitizing, followed by a water quench. Full solution of carbides requires solution treating at 30–50 °C above A_{CM}. The pouring temperature is usually less than 1470 °C to prevent an excessively coarse grain size and minimize chemical segregation [61]. The typical solution heat treatment temperature is around 1010–1120 °C. A low heating rate is required to prevent internal cracking, and a high quench rate is preferred in order to prevent carbide formation. The outstanding mechanical properties of Hadfield steel are inherent toughness and an exceptional strain hardening capability, leading to a tough, and wear- and deformation-resistant steel under certain operating conditions. It is usually the wear-resistant material of choice when impact loading makes it impossible to employ materials like white cast irons. The typical mechanical properties are summarized after Dastur et al. [63] in Table 1.

Table 1
Mechanical properties of Hadfield steel (1.0–1.4 %wt. C, 10–14 %wt. Mn).

0.2% Offset Yield Strength	379 MPa
Ultimate Tensile Strength	965 MPa
Elongation	50%
Reduction of Area	40%
As Quench Hardness	190 HB
Hardness at Fracture	500 HB
Charpy V-Notch Impact at 22 °C	169 J
Charpy V-Notch Impact at −196 °C	7 J

2.1. Single crystal deformation characteristics

The hardening mechanism of Hadfield steels is related with deformation twinning, dislocation slip and their interaction [11]. In an earlier work on polycrystalline material, Adler, Olson and Owen [15] noted the significant similarity in the twinning kinetics between the Hadfield steel and the low stacking fault energy Co-33Ni alloy, studied by Remy [64], both deformed in tension. Specifically, they compared the twin volume fraction as a function of true plastic strain. Polycrystalline stress-strain response is an outcome of the aggregate behavior of all grains combined. By contrast, the single crystal hardening behavior is strongly orientation-dependent due to the strong anisotropy of available straining planes and directions [65]. Although a single crystal may not have immediate industrial application, it can help understand the inherent deformation propensity of an isolated grain, free of grain boundary and texture effects. Karaman et al. reported detailed mechanical characterizations and microstructure characterizations on single crystals [22,23,66]. In Fig. 3, compressive and tensile stress-strain responses are compared, where the strong orientation dependence of flow stress can be noted. By studying microstructure through electron microscopy, they found evidence of twinning- and slip-dominated deformation mechanisms [2,22,23,66] under different loading orientations. The middle schematic in Fig. 3 summarily expresses their findings on the correlation among the predominant deformation mechanism (slip or twinning), the single crystal orientation and loading direction (tension or compression). For instance, $\langle 111 \rangle$ tension and $\langle 001 \rangle$ compression result in twinning-mediated deformation. On the other hand, slip-based plasticity (with no twinning) is noted for $\langle 123 \rangle$ and $\langle 001 \rangle$ tensile as well as $\langle 123 \rangle$ and $\langle 111 \rangle$ compressive loads. Transmission electron microscopy (TEM) evidence of deformed microstructure for individual cases is presented in Fig. 4.

Twinning essentially leads to an increased volume fraction of interfaces, which in turn act as barriers to slip motion. This situation is analogous to grain refinement, which gives rise to strengthening attributes. The shear strains associated with twinning accounts for the ductile response. The concurrent slip and twinning underlie the high toughness of Hadfield steels. Relative predilection of slip and twinning may, however, differ significantly from grain to grain depending on the maximum Schmid factors operative on either system. Predominance of a certain deformation mechanism is noted for single crystals loaded along different crystallographic directions.

2.2. Effect of nitrogen alloying

Alloying with nitrogen is recognized for increased strength benefits in the steel technology [67–72]. The elemental nitrogen is a well-known austenite stabilizer. Moreover, the prospect of substantial solid solution hardening has also remained an attractive feature. There are studies exploring the nitrogen-induced hardening effects in the single crystals of austenitic

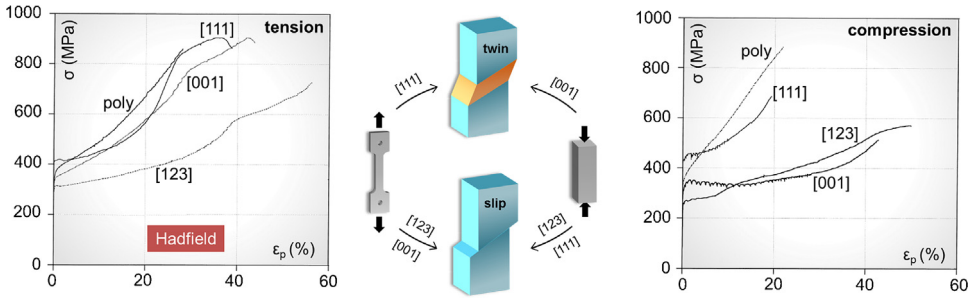

Fig. 3. Summary of tensile and compressive responses of single crystal Hadfield steels, which result in either slip- or twinning-dominated plasticity depending on the loading direction and crystal orientation [66].

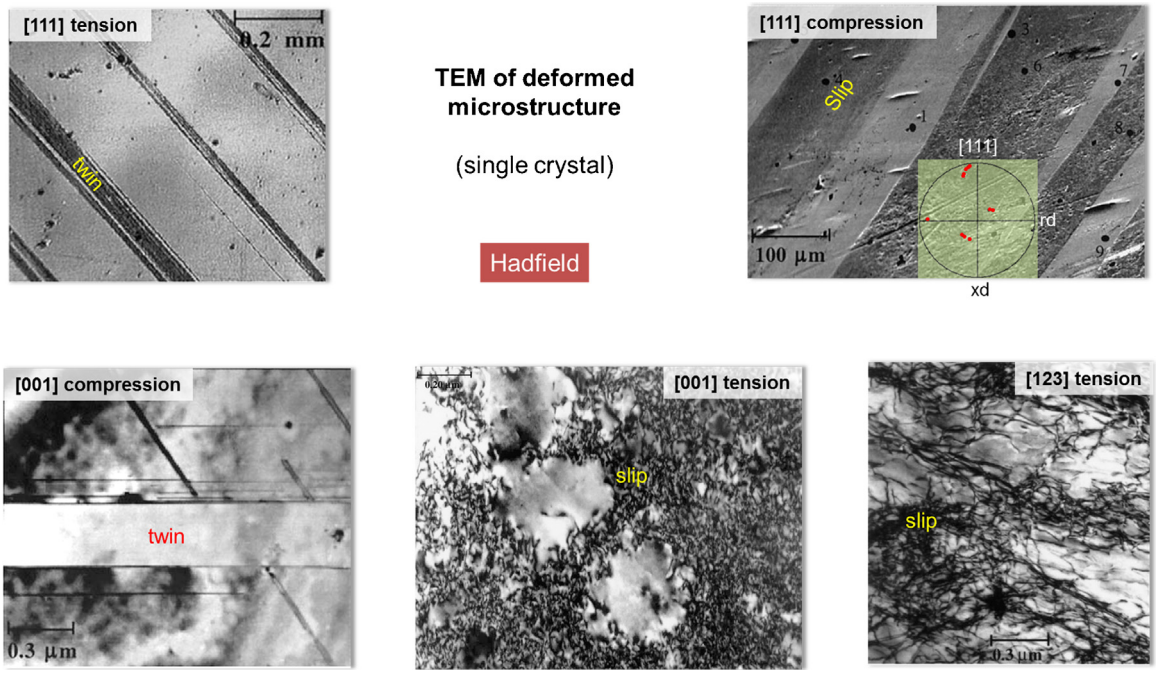

Fig. 4. TEM studies on the deformed microstructure of single crystal Hadfield steels [66].

stainless steels, for example, by Chumlyakov and co-workers [73–75]. The nitrogen addition was reported to have significant impact on the toughness of the Hadfield steel single crystals as well [17,76]. From the standpoint of solid solution effects, nitrogen atoms, compared to carbon, have stronger affinity for manganese atoms as noted by Berns et al. [77]. Due to considerable presence of Mn in Hadfield steel crystals, the propensity of creating nitride precipitates is high, which is substantiated through microstructure characterization [76].

Canadinc et al. [76] studied single crystals alloyed with 0.05 wt% and 1.06 wt% nitrogen under compression. They noted considerable increases in the CRSS levels as well as the strain hardening coefficients as a function of composition (Fig. 5). The trends were consistent for a number of loading orientations, whereby compressive loads along the ⟨111⟩ orientation led to the greatest strengthening. The average CRSS value for single crystal Hadfield steels with no added nitrogen was determined to be around 120 MPa. For 0.05 wt% N case, the CRSS is raised to 140 MPa (averaged). For the highest N concentration studied (i.e. 1.06 wt%), an increased value as high as 300 MPa (approx.) was noted. From the stress-strain curves, increasing N content was associated with a gradually decreasing ductility. Nonetheless, due to substantial strengthening benefits, an enhanced degree of toughening was noted on the whole. Upon examining the deformed microstructure, the 1.06 wt% nitrogen-alloyed materials were reported to have impenetrable nitride precipitates, which posed considerable barriers to free dislocation glide. It was concluded that the N-induced solid solution hardening governs the stage I hardening whereas the precipitate-induced flow resistance is responsible for enhanced stage II strengthening effects. Through out the inelastic deformation regime, the plastic flow was dominated by slip-twin and twin–twin interceptions. Considering samples of polycrystalline microstructure, Iglesias et al. [17] also examined the effects of N-concentration on the Hadfield steel properties. Using optical micrographs, they reported occurrence of slip-twin interactions in multiple grains, which contributed to the overall constitutive response of the material. From their results, it was also inferred that the higher N content would give rise to increased hardening attributes.

2.3. Role of aluminum addition

Addition of Al has significant effect of the mechanical responses and the associated deformation mechanism(s) of Hadfield steel [18,20,21,78–81]. In polycrystalline samples, Zudeima et al. [80] reported an increased strain hardening rate and a high-stress

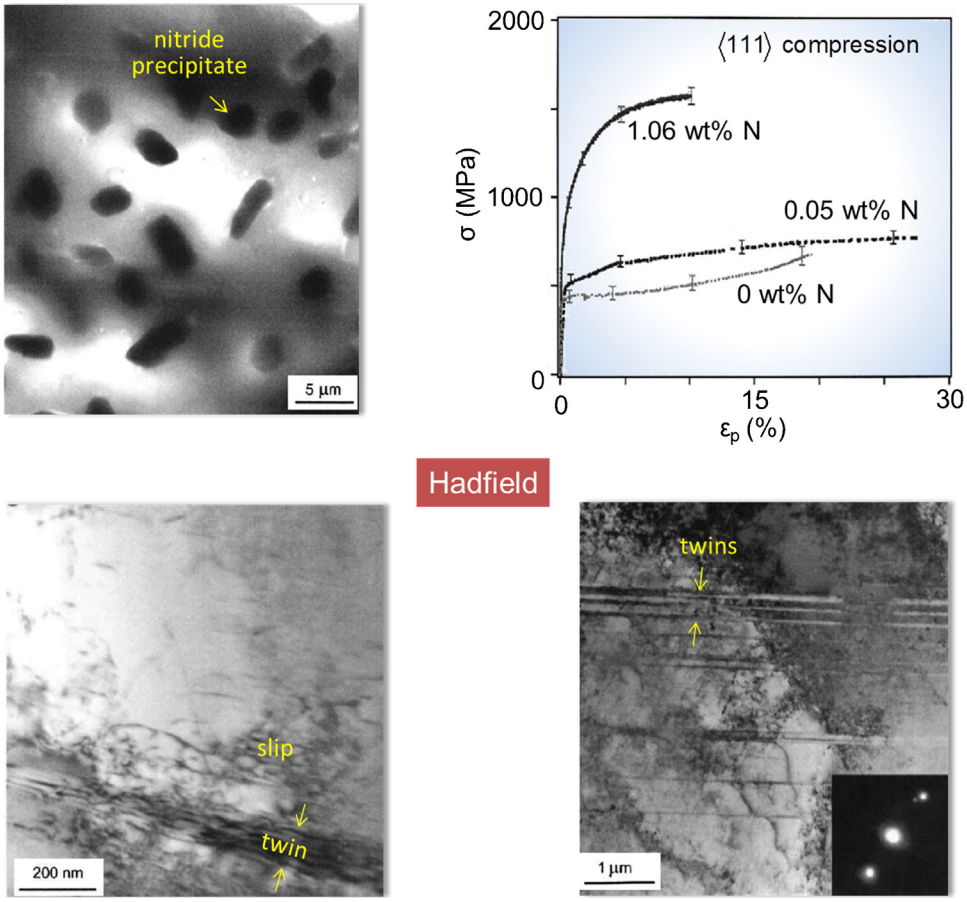

Fig. 5. Stress-strain responses of various N-alloyed Hadfield steels and the associated deformed microstructure [76].

abrasion resistance as a result of Al alloying. They noted that the Al served to raise the stacking fault energy, thereby suppressing twinning propensity. Specifically, an optimum Al content was noted beyond which the foregoing effects subsided. By studying single crystals, Canadinc et al. [78] noted the prevalence of coplanar dislocation morphology, which led to the formation of high density dislocation wall oriented along ⟨111⟩ direction. These walls reportedly constitute further obstacles to dislocation motion as the deformation progresses, giving rise to high hardening rates. Their results are summarized in Fig. 6. Similar conclusion was drawn by Astafurova et al. [79,82]. Moreover, they investigated ductile-to-brittle transition behavior of Al-alloyed Hadfield single crystals [19]. Nonetheless, they noticed minute twinning activities followed by significant slipping. Similarly, Abbasi et al. [18,81] observed high plastic strength with a predominant suppression of twinning, although evidence of micro-twinning phenomena in the later stage of deformation was noted. The final fracture surface was reportedly characterized by somewhat brittle morphology as noted by Astafurova et al. and Abbasi et al. [18,79,81,82].

2.4. On strain-rate sensitivity and other properties

Rate sensitivity of the deformation response is quite common in metallic materials, and especially in steels. Strain rate sensitivity (SRS) in steels usually refers to the phenomenon when the flow stress increases for the same strain levels concomitant with the rate of deformation, which is capable of significantly affecting the work hardening response and capacity during deformation [83]. Thus, understanding the SRS of an alloy is of utmost importance especially for manufacturing purposes [84], such that an unexpected outcome does not prevail as a result of SRS-related behavior during forming.

For a pure metal deforming by slip only, the explanation of SRS, i.e. the increase of flow stress with increasing strain rate, can be as simple as the enhanced forest hardening due to increased energy facilitating the formation and glide of dislocations at higher rates of deformation. However, both the occurrence and understanding of SRS in multi-element alloys with complicated micro-deformation mechanisms, such as the Hadfield steel, require further elaboration.

Despite having been investigated by several researchers for decades, there is still controversy regarding the cause of the unusual strain hardening response of Hadfield steel. This superior steel, which exhibits high wear resistance combined with high ductility and strength, possesses an inherent toughness and an exceptional work hardening capability [15,63,85,86]. The lattice structure is face-centered cubic (fcc) at room temperature [12], mainly due to chemical stabilization of austenite by carbon (C) and manganese (Mn) in the microstructure [83]. Initially, the unusually high strain hardening coefficients of Hadfield steel have been attributed to the formation of twin boundaries that provided strong barriers to dislocation motion [11,15,22,23,66,87]. Interruption of the glide dislocation path by stacking faults [14] is among other reasons forwarded to explain the unusual strain hardening of the Hadfield steel. In addition, Owen, Dastur and colleagues claimed that dynamic strain aging (DSA) is the mechanism underlying the rapid strain hardening exhibited by Hadfield steel (HS) [12,63]. It was also shown that alloying of HS with aluminum (HSwAl) further increased the strain hardening rate by enhancing the formation of high-density dislocation walls (HDDWs) and their

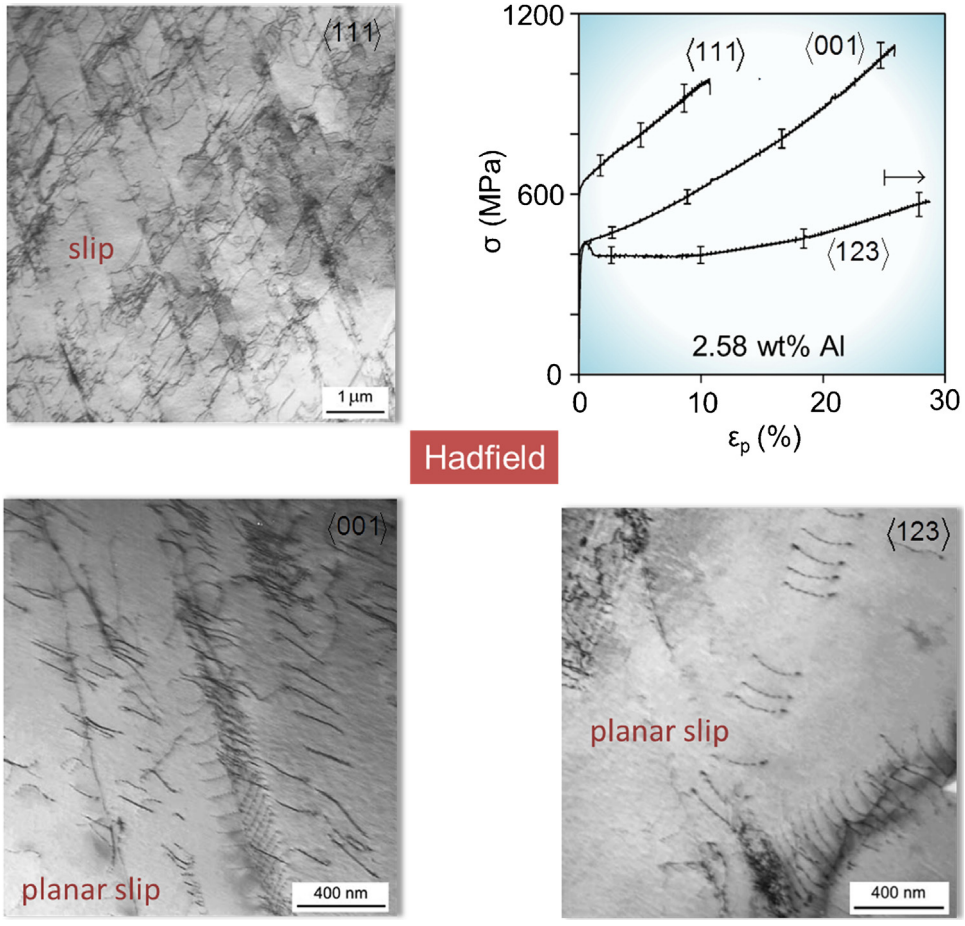

Fig. 6. Constitutive behaviors of Al-alloyed Hadfield steels and the TEM evidence of deformed microstructure [78].

interactions with active slip systems, as demonstrated in transmission electron microscopy (TEM) investigations [78].

Dastur and Leslie [63] were the first researchers to link the rapid strain hardening of Hadfield steel to dynamic strain aging (DSA), through a study that investigated the tensile deformation response of Hadfield steel polycrystals within a temperature range of −25 to 300 °C. Low work hardening rates were observed at low temperatures despite twin formation, and high strain hardening rates were evident at high temperatures without any twin formation. Based on these observations, Dastur and Leslie [63] claimed that DSA, brought about by the reorientation of carbon members of Mn-C couples in the cores of dislocations, was the primary cause of rapid strain hardening in Hadfield steel. The study, however; was confined to experimental observations and theoretical explanations, and a model to help explain the theoretical ideas was not forwarded.

Another investigation reaching the same conclusion was carried out by Owen and Grujicic [12]. They attributed the DSA, which is the major cause of rapid strain hardening in Hadfield steel, to the enhanced C diffusion due to increased dislocation density. A model was proposed, which took into account the change in the probability of possible metal-interstitial atom pairs, led by the destruction of the local order due to the passage of a dislocation. Slip induced chemical energy changes, which are reflected through the number and distribution of nearest neighbor chemical bonds, leads to the rapid strain hardening observed in Hadfield steel. The model demonstrated the contribution of DSA to the overall hardening; however; the results reflected the deformation induced statistical changes in the distribution of metal-interstitial atom pairs, and the corresponding chemical energy changes.

Whereas there are a very limited number of studies focusing on the DSA in Hadfield steel, DSA and rate sensitivity in metallic alloys have been the focus of attention in many works. The works by Cottrell et al. [88,89], Van den Beukel et al. [90,91], Louat [92] and McCormick et al. [93–95] have laid out the fundamentals and important details of the DSA. Theoretical framework was established in detail, and numerical models were utilized to test the theories. Nevertheless, the focus of the numerical simulations was confined mostly to the statistical analysis of shear instability and stress drops during deformation, as well as the Portevin Le Chatelier (PLC) effect. Some works included numerical simulations of stress dependence on dislocation position on the atomic scale [88] or stress-time response [95], however; neither these works nor others to follow have presented a thorough analysis targeting the rate sensitivity of the macroscopic deformation response and its prediction.

Canadinc et al. [83] studied the role of DSA on the tensile deformation response of Hadfield steel, such that the experimental results demonstrated a clear negative strain rate sensitivity (NSRS) within the strain rate range of $1\times10^{-4}\,s^{-1}<\varepsilon<1\times10^{-1}\,s^{-1}$ (Fig. 7). In particular, within this range of deformation rates, the flow stress was observed to decrease significantly, despite the increasing strain rate. The digital image correlation (DIC) studies demonstrated that the strain fields within the gage section exhibit a significant inhomogeneity, such that the strains notably vary within the matrix, as also evident from the striations in the flow curves that are typical of rate sensitive materials. However, unlike in other alloys, such as aluminum alloys [96–98], PLC band formation was not observed in Hadfield steel, as evidenced by the DIC results. Comparison of strain localization for two different

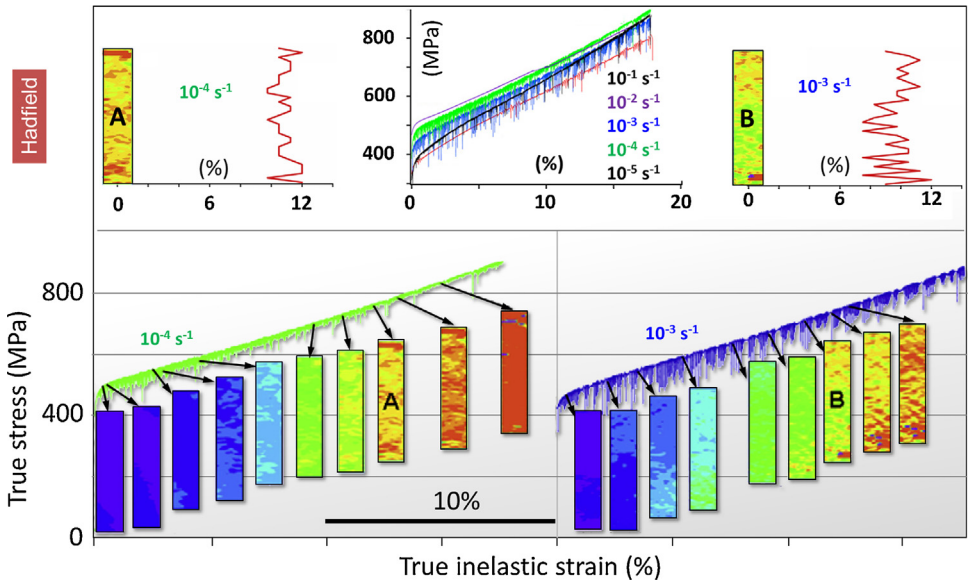

Fig. 7. Experimental results demonstrating the NSRS of Hadfield steel and the detailed DIC analysis demonstrating the NSRS imposed instabilities throughout the gage sections of samples for selected strain rates [83].

rates ($10^{-4}\,s^{-1}$ and $10^{-3}\,s^{-1}$) for selected DIC snapshot (designated "A" and "B") is presented in the inset of Fig. 7. The strain variation along the gage length of the specimen is also shown. Note that the degree of local non-uniformity is higher in the $10^{-3}\,s^{-1}$ case, which is also evident from the maximum amplitude of striations in the flow curve at this strain rate.

The reason for the observed instability throughout the gage section was associated with a competition between the DSA and forest hardening depending on the strain rate [83]. DSA is attributed to the pinning of mobile dislocations arrested at obstacles by the solute atoms diffusing within the matrix [91]. When the dislocation glide is hindered by obstacles, there is an elapse of time before the dislocations overcome the obstacles. The average time the dislocations stay arrested at obstacles throughout the matrix is defined as the waiting time, t_w, which is proportional to the density of mobile dislocations (ρ), the dislocation mean free path (L), and the inverse of strain rate ($1/\dot{\varepsilon}$). The Orowan equation [91,93,94] defines the waiting time as:

$$t_w = \rho b L/\varepsilon \qquad (1)$$

Where "b" denotes the magnitude of Burgers vector. During the waiting time, solute atoms might diffuse into the arrested dislocations, leading to DSA [91]. One can picture the rapid strain hardening of Hadfield steel as a superposition of contributions from slip and DSA [11,12,14,15,20,22,23,63,66,78,87,99], yet the strain rate dictates the cooperation of these factors and the respective importance of their contributions to the overall hardening. Specifically, as the ε increases, t_w decreases, leaving less time for C atoms to age the interrupted dislocations. Nevertheless, the increasing strain rate also increases the energy of the system, providing more energy to C atoms, eventually enhancing the ability of C to diffuse within the matrix and pin the arrested dislocations. Experimentally, the macroscopic effect of this competition between the diffusivity of C and the aging of blocked dislocations by C is observed in the form of an overall decrease in the strength levels, NSRS (negative strain rate sensitivity), and the accompanying instabilities (Fig. 7). The increased magnitude of (local) stress drops and the loss of strength despite the increasing ε within the NSRS range clearly demonstrate the associated instability owing to the elevated state of energy in the system. Once the ε is beyond the NSRS range, the NSRS diminishes and a more stable deformation response with stress drops much smaller in magnitude are evident.

The explanations forwarded by Canadinc et al. [83] based on their experimental results were recently supported by a multi-scale model proposed by Bal et al. [100]. In particular, the diffusivity of carbon depending on the strain rate was successfully modeled at atomistic scale based on Uslu et al.'s work on the mobility of hydrogen atoms within iron matrix [101], such that the contributions of shear stresses arising from the pinning of dislocations by carbon atoms to the overall shear stress (facilitating the glide of dislocations on active slip systems) were computed. This additional contribution was then scaled up to the slip system level, and both the deformation response of the material and the repeating serrations due to instability related to NSRS were predicted [100] (Fig. 8).

The deformation response of Hadfield steel beyond the NSRS range has recently been investigated owing to the load bearing potential of this material implied by its unusually high strain hardening capacity. Specifically, the impact response [102–104] and the hardening behavior when subjected to explosive loading [105] were investigated both experimentally and numerically. The findings of these works revealed that Hadfield steel features nano-twins forming within primary twins [102], providing an additional mechanism for the continuation of plastic deformation under high-velocity loading, and thereby increasing the load bearing capacity under impact loading. These recent findings and the newly proposed multi-scale modeling approaches predicting the deformation response by incorporating microstructure [103,104] and triaxiality [103] would be useful for the study of high-velocity deformation response of TWIP steels, which have already attracted a significant attention [38,102,106–109].

2.5. Future promises: alloy design, TWIP steels and high entropy alloys, advanced modeling

A significant volume of scientific work carried out on Hadfield steels has focused on many aspects of the formability and deformation response of these materials: micro-deformation mechanism interactions, alloying effects, solid solution hardening, microstructure evolution, dynamic strain aging, negative strain sensitivity and more. Both experimental results and theoretical

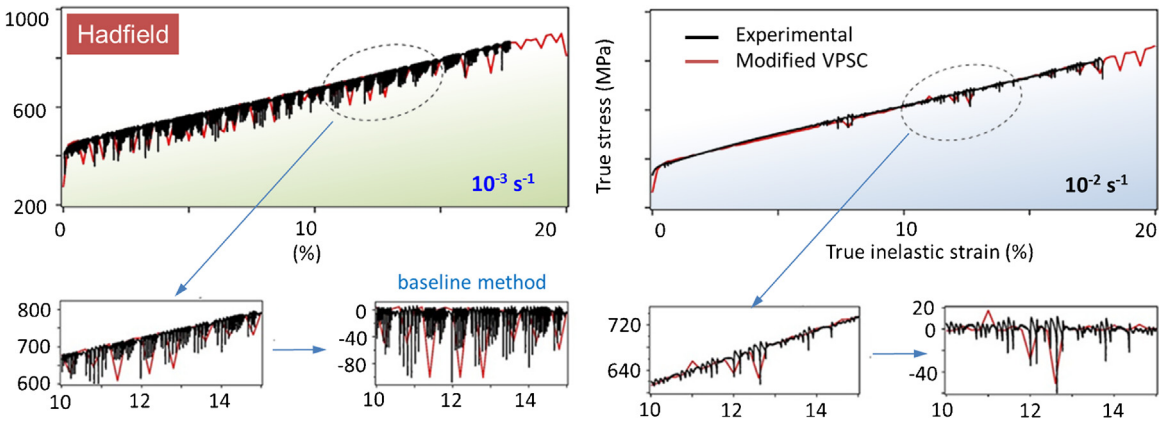

Fig. 8. Results of recent multi-scale simulations that can predict the role of DSA on the NSRS of Hadfield steel [100].

frameworks have helped us understand the individual roles of micro-deformation mechanisms and various microstructural features on the formability and strain hardening response of these materials. In light of the fact that much has been uncovered about Hadfield steel itself, the corresponding findings and models proposed to predict the deformation response of this alloy indeed altogether form the basis for the greater framework of alloy design for improved performance and durability. In particular, the scientific works mentioned herein clearly showed that Hadfield steels possess a very complicated microstructure with both slip, twinning and various interactions of these mechanisms with other features being simultaneously active. The thorough set of experiments carried out on this material and especially the crystal plasticity models provided the opportunity to distinguish between the individual contributions of multiple parameters governing the strain hardening response. This, in turn, opened a venue to tailor the mechanical properties of the material to desired performance criteria during forming or service, for instance, by alloying or optimizing processing parameters, such as temperature and rate of deformation, in order to facilitate deformation by desired mechanisms. Since many of the mechanisms and the corresponding microstructural interactions active in Hadfield steels also prevail in other classes of steels and metallic materials, the knowledge built on Hadfield steels constitutes the basis of alloy design framework for several materials.

A good example to this argument is the development of TWIP steels. The introduction of TWIP steels followed the advances in Hadfield steel: the understanding of the role of Mn content on the stacking fault energy and the microstructure of Hadfield steels led researchers to the discovery of TWIP steels [33,34,110–113], which deform by similar micro-deformation as Hadfield steel [114,115], yet TWIP steels are superior to Hadfield steels in terms of some mechanical properties. One can notice that the research on the deformation response and formability of TWIP steel advanced much faster as compared to that of Hadfield steel, which is partially owing to the existing knowledge on Hadfield steel. In a similar fashion, the findings on the microstructure evolution of Hadfield steel is expected to significantly support the progress of research on HEAs since even the earlier works [116] on these materials have already shown the similarity of the micro-mechanisms facilitating the deformation in HEAs and Hadfield steels.

From the discussions heretofore, it is evident that there exist significant literature on the mechanical and microstructural characterizations of the Hadfield on experimental grounds. In summary, a concurrence of slip, twinning and their interactions with obstacles decide the fundamental constitutive attributes. Phenomenological models have been capable of predicting the empirical response, thereby paving the way for engineering analysis, say, using finite element simulations [117,118]. The next question that arises is how to further leverage the unique deformation feature at the microscopic lengthscale to achieve the desired engineering attributes. For example, role of a particular alloying element (e.g. N, Al) has been found to be profound through exhaustive experimentations [20,76,78]. Typically, discovery of this nature requires significant trial and errors based mainly on the thermodynamics and the knowledge of phase diagram. Newly emerging computational methods can potentially complement the devising process of new alloys [119]. For instance, quantum mechanics based tools have proven useful in unearthing the subtle effects of adding solute atoms to the base metal under the defect-free crystal condition [120,121]. Such predictive tools have also demonstrated efficacy in modeling the stacking fault energy [122], which has a significant role in determining slip versus twinning as observed empirically [123]. Density functional theory (DFT) based calculations can be a useful proving ground for testing various hypotheses on alloy compositions and lattice attributes. This can help formulate how to achieve the desired level of stacking fault energies such that correspondingly greater/lesser degree of twinning or slip dissociation predilection. This can potentially contribute to the phenomenological twinning models, where the stacking fault energy has remained a major input [124]. Similarly, curve-fitted potential based molecular dynamics simulations are now being explored to discover various deformation mechanisms in a single grain lengthscale [125–127]. It remains to be seen how these promising avenues of research yield interesting insight into developing novel alloys with superior properties.

3. Twinning induced plasticity (TWIP) steel

Recently, considerable effort has been spent on the development of light-weight metallic materials in order to engineer more energy efficient structures without sacrificing safety by increasing the specific strength of the materials [4,33]. Despite the significant improvements in mechanical performance of light-weight magnesium (Mg) and aluminum (Al) alloys [128–132], recent developments in the field of advanced high-strength steels have paved the way for utilizing steel components with reduced weight yet high toughness. While aluminum and magnesium alloys continue to be the best known and mostly utilized light-weight alloys, recent studies within the last decades led to the development of new steel grades with a high specific strength [4,33,133–135]. For instance, dual-phase, complex-phase and boron-alloyed steels are currently utilized in the making of automobile components, such as B-pillars and other crash relevant structures, since these materials both possess high specific strength values and demonstrate formability into complex geometries [136–138].

The metastable high-manganese austenitic steels falls into this category [4,33,139–141]. These steels do not undergo phase transformation upon processing or cooling, but rather need to attain a certain energy level to transform, which can be facilitated by mechanical deformation [4], such as in the highly-strained regions of the material (e.g. necking zones). During monotonic deformation, this class of steels can demonstrate two different mechanisms of strain hardening: martensitic transformation, which is referred to as transformation-induced plasticity (TRIP), or twinning, also known as twinning-induced plasticity (TWIP) [4,33]. It has been shown that the mechanism of strain hardening in this class of steels can be tailored by adjusting the content of alloying elements, such as manganese (Mn) and aluminum (Al) [139–141]. The alloying content of the steel has a direct influence on the stacking fault energy (SFE) of the material, which dictates the activity of deformation mechanisms throughout deformation [78]. Specifically, TRIP steels are characterized by a very low SFE, while TWIP steels possess higher SFE [4,33]. However, a clear distinction between TRIP and TWIP effects cannot be made easily, as a high-Mn steel with a medium SFE may exhibit both [33,139].

TRIP steels and TRIP-assisted multiphase steels have been developed much earlier than TWIP steels, and thus, more information is available on their processing and mechanical properties [142–145]. TWIP steels, on the other hand, have received some attention only recently, where the focus has been placed mostly on their processing, and monotonic deformation response and the corresponding microstructure evolution [4,33,139]. It has been shown that twinning is prevalent in the necking zones in TWIP steels under monotonic loading, providing added strength in these areas [4,33], such that the deformation proceeds in the surrounding areas, allowing further straining of the sample due to prevention of localized damage [4,33].

In the light of these recent developments, high-manganese (Mn) austenitic steels have become an alternative to Mg- and Al-alloys, especially in automotive, railroad and mining industries [2,38,146,147]. Earlier studies on high-Mn austenitic steels focused mainly on Hadfield steel [12,16,32,63,66,78,99,139,148–153], which could be considered as the precursor material to new-generation high-strength steels. The findings of the works focusing on the stacking fault energy (SFE), rapid strain hardening, microstructure evolution and strain rate sensitivity of Hadfield steel led to the introduction of relatively higher Mn containing (13–30 wt.% Mn) steels, and eventually the development of TWIP steels [33,34,110–113]. This class of steels possess an excellent combination of high strength and ductility (Fig. 2) in comparison with other classes of conventional steels; typically, strengths up to 1500 MPa, elongations up to 90%, and outstanding impact toughness ranging from 90 to 120 J/cm^2 at high strain rates have been reported for TWIP steels at various temperatures [33,34,110–113]. In addition to these superior mechanical properties, TWIP steels possess relatively lower density (7.3 g/cm^3) and much higher energy-absorption capacity (0.5 J/mm^3) than conventional steels, with typical density and energy absorption values of 7.8 g/cm^3 and 0.25 J/mm^3, respectively [4,33,112,113,154].

3.1. Micro-deformation mechanisms governing the strain hardening in TWIP steels

Many of the earlier investigations reported that twinning accompanied by additional micro-mechanisms, such as stacking faults, dynamic strain aging (DSA) and slip-twin interactions, dominates the deformation response of TWIP steels, where the role of dislocation glide remains rather limited in comparison [28,155–157]. In particular, at the onset of plastic deformation, twins start to nucleate, and the volume fractions of nano- and micro-scale twins increase during plastic deformation, forming twin boundaries of different magnitudes. In Fig. 9, a case study is presented, which summarizes the relationship between the mechanical properties and microstructure evolution after Mosecker et al. [158]. We note that for a wide range of

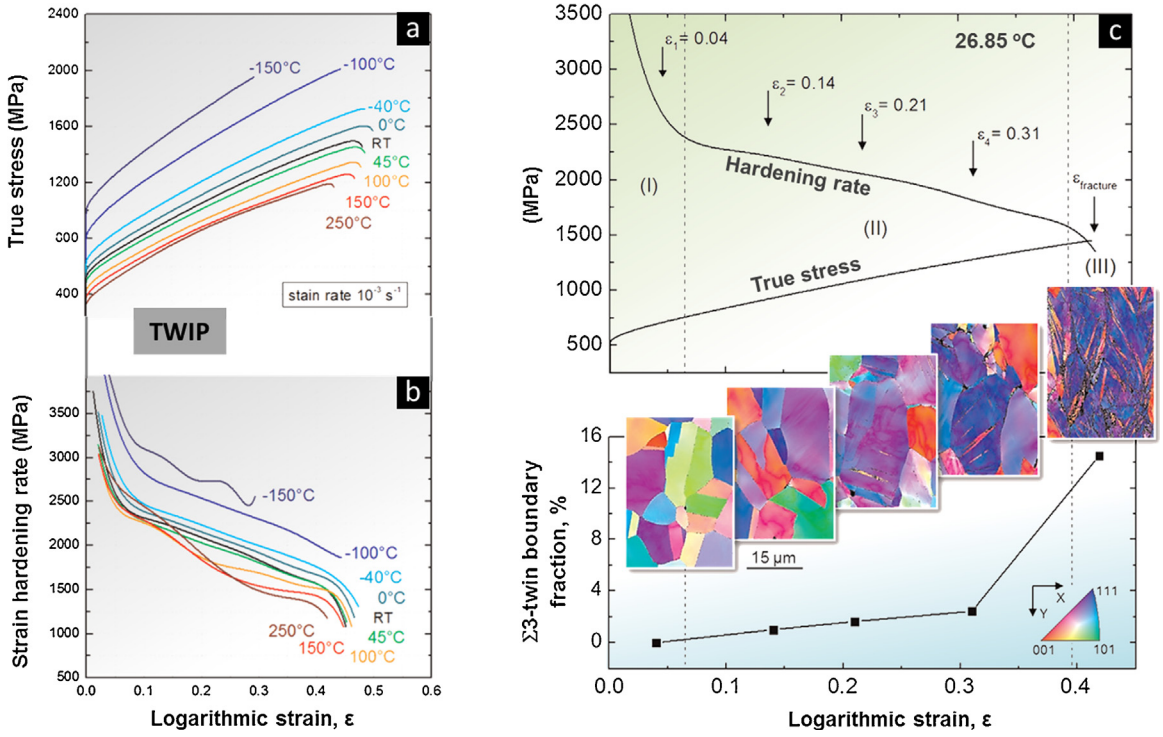

Fig. 9. (a) True stress-strain responses at various temperatures, (b) evolution of hardening rate at the corresponding strain levels, and (c) (top) stress-strain behavior at 300 K with the associated hardening rate changes, (bottom) twin volume fraction increasing exponential with increasing strain (EBSD insets showing the grain segmentation due to evolving twinning) [158].

temperatures, the ductility of the TWIP steels is remarkable. The hardening rate varies in a similar manner for the same temperature window (from −150 °C to 250 °C), which indicates a consistent variation of deformation stages (marked as I, II and III). The underlying reason is rooted upon the uniformity of the deformation mechanism, which is dominated by twinning at higher stress preceded by dislocation activities (as evident from the inset EBSD images). Notice that the volume fraction of twins rises in an (nearly) exponential manner.

Evidence of mechanical twinning as a result of cold rolling is reported by Vercammen et al. [26] as in upper inset of Fig. 10. The lower inset showcases a study where micro-twins were observed to intercept relatively larger twins as noted by Chen et al. [159]. A closer inspection of the twins in a polycrystalline microstructure is presented in Fig. 11(a) using ESBD scan as reported by Gutierrez-Urrutia and Raabe [24]. Fig. 11(b) shows the TEM evidence of twin lamella intercepted by stacking fault (SF). In Fig. 11(c), dislocation pileups at the planar interface can be noticed [158].

In materials that are only deformed by dislocation glide, the mean free path of dislocations is a function of grain boundary (GB) density and dislocation–dislocation interactions. However, in the case of TWIP steels the twin boundaries formed within the microstructure also play a crucial role. Specifically, the mean free path of dislocations is reduced by the increasing twin boundaries, which act as strong obstacles against dislocation glide and bring about the noticeable strain hardening observed in TWIP steels [18,28,139,155]. This is known as the TWIP effect, which is triggered at low or medium SFE values (12–35 mJ/m^2) [123]. Based on a thermodynamics model, Song et al. [160] examined the variations in SFE level as a function of the alloy composition (Fig. 12). Changing level of SFE bears significant implications regarding the dominant deformation mechanism. For instance, very low stacking fault energy promotes twinning while high SFE means plasticity mediated by full dislocations. The intermediate value of SFE is associated with prevalence of extended slip (connected by a stacking fault plane). The observed effects could be traced back to how defects in the discrete lattice would be nucleated as a result of the SFE magnitude. As observed in the deformed microstructure, plasticity in TWIP is typically initiated in the form of pervasive slip followed by twinning and then slip-twin, twin–twin interactions.

Both the TWIP effect and microstructural interactions suspend the onset of necking since they are obstacles for dislocation glide, and as a result, high ultimate tensile strength values with extraordinary ductility are achieved before necking in high-manganese austenitic TWIP steels [37,107,112,113,161]. However, if the mobile dislocation density is not large enough or the mean free path of dislocations is not short enough to provide for the critical twin nucleation stress, growth of existing twins is favored over the nucleation of new ones. As a result, the volume for microstructural interactions becomes smaller, and therefore, easier dislocation glide takes place, eventually leading to softening of the material [162].

3.2. Deformation of TWIP steels at high strain rates

The aforementioned superior mechanical performance of TWIP steel has been observed in various investigations, which focused on

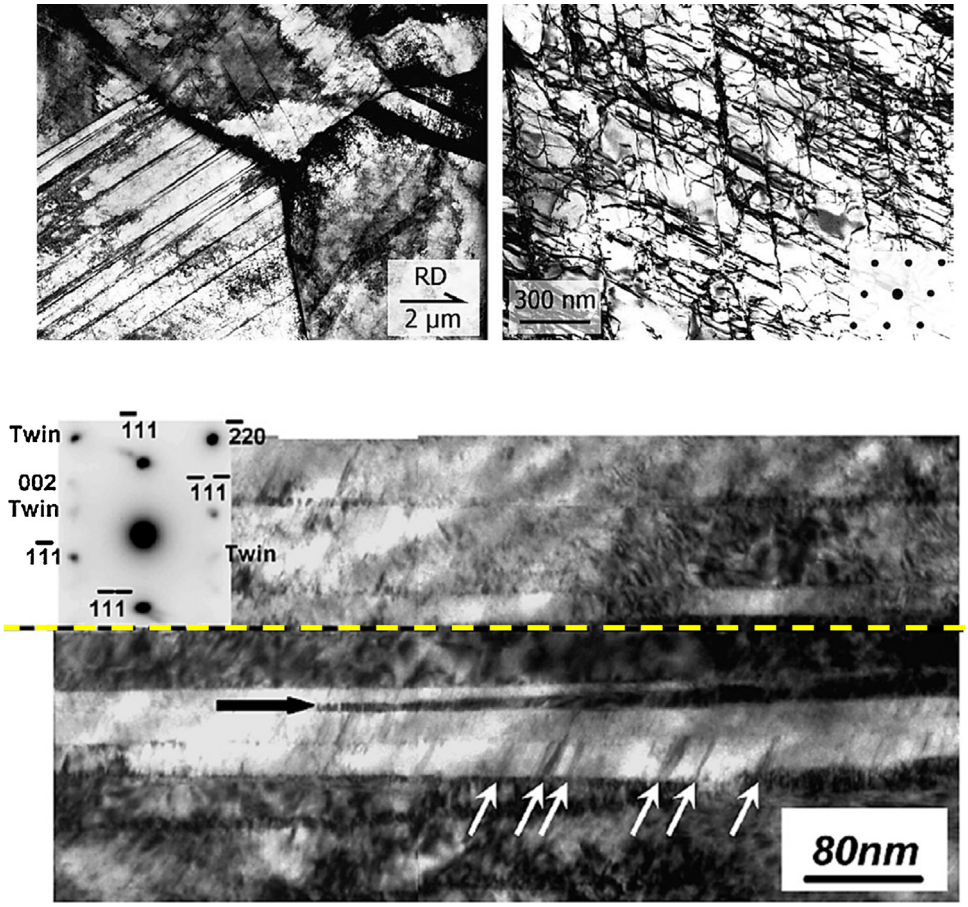

Fig. 10. (Top left) Evidence of mechanical twins in the polycrystalline microstructure of a cold-rolled TWIP sample; grains, not having twins, contain dislocation networks [26]. (Bottom) Parallel twins (indicated by dark arrow) which are internally faulted by micro-twins (white arrows) [159].

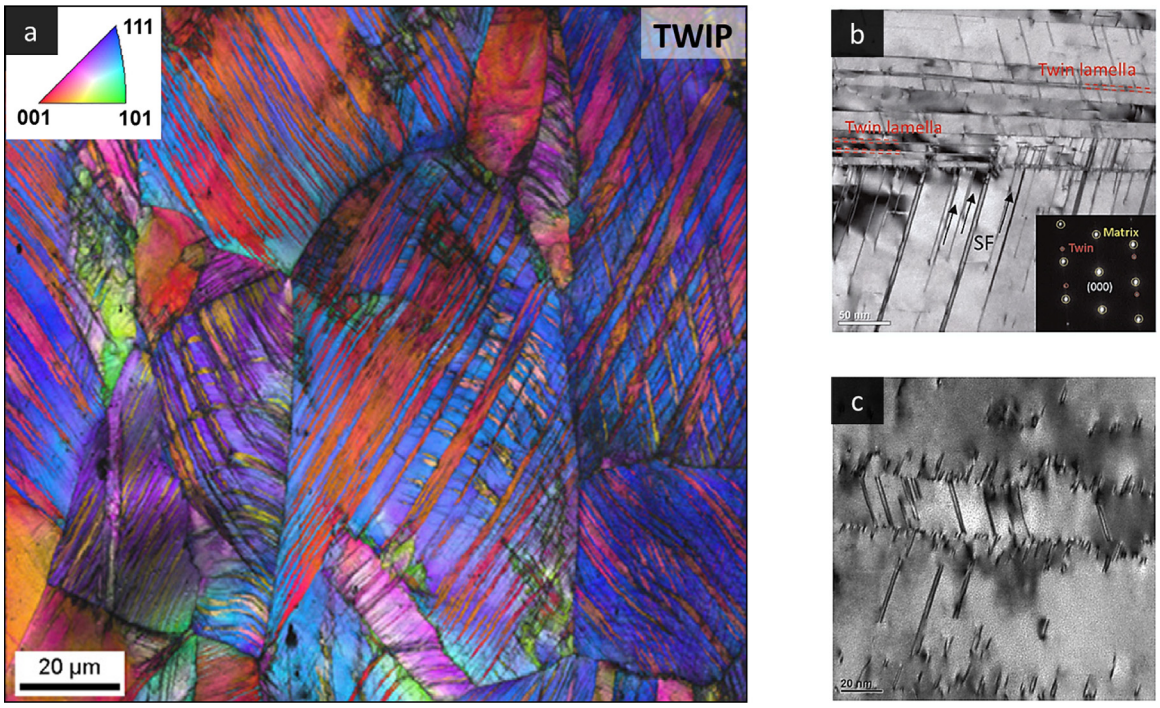

Fig. 11. (a) EBSD map of TWIP deformed under tensile loads showing pervasive twining activities in each grain [24], (b) blocking of extended stacking faults (SF) by nano-sized twin lamella [158], and (c) dislocation blocked by planar defects [158].

tensile properties [37,38,107,163,164], deformation behavior and the corresponding micro-deformation mechanisms [113,161,165–167], fatigue [35,112,168–172], effects of alloying elements [4,173–176] and fracture [31,176] of high-Mn TWIP steels. Consequently, it was reported that TWIP steels have high strain hardening capacity due to twin-slip interactions under tensile or compressive loading.

As opposed to static, quasi-static or cyclic tensile/compressive loading, high strain rate impact loading enhances only one

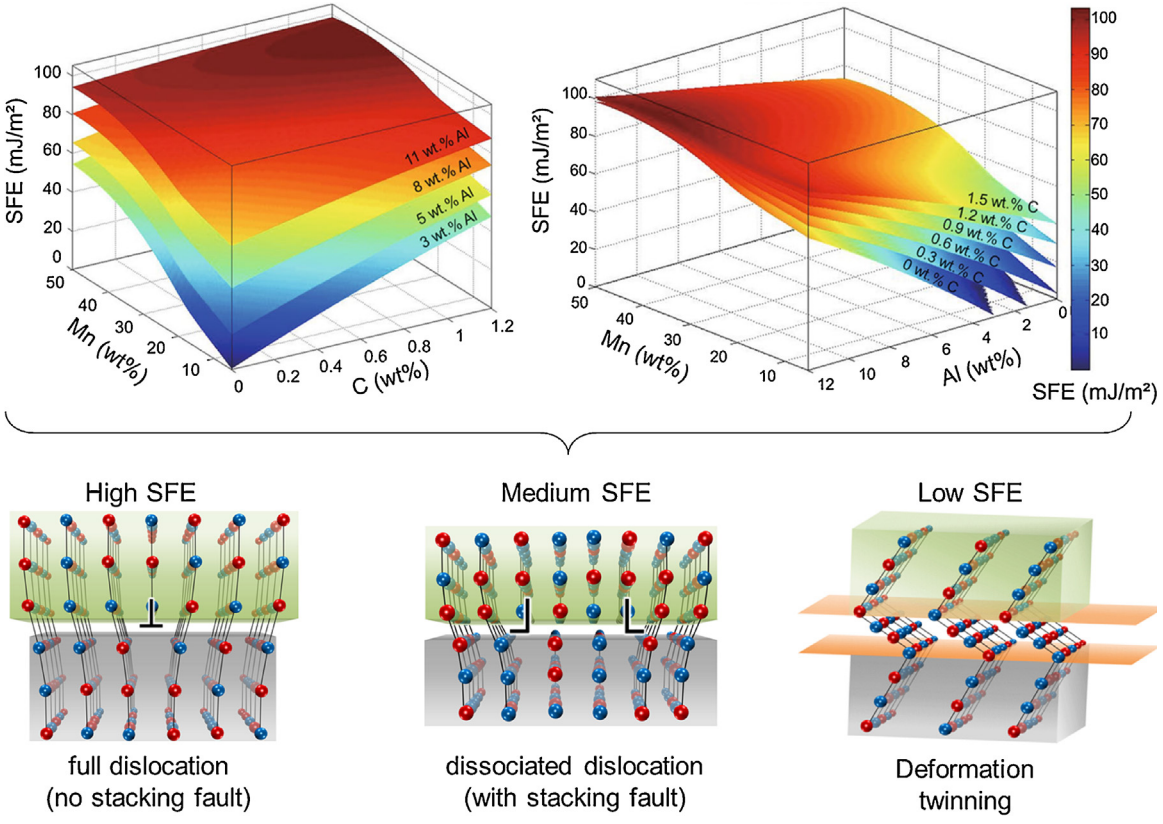

Fig. 12. Role of Al and C content on the stacking fault energy (SFE) levels as predicted by Song et al. [160] based on thermodynamic assumptions.

deformation mechanism rather than their complex interactions, a fact which enables a more comprehensive and straightforward understanding of the microstructural evolution of high-Mn steels [177]. A limited number of studies also investigated the microstructure evolution of high-Mn steels under high-strain rate deformations, such as impact loading, which induces the micro-deformation mechanism interactions due to the complexity of the applied loading [146,177]. For instance, Wen et al. [146] and Toker et al. [177] reported the deformation behavior of a new generation high-Mn austenitic steel under impact loading, however; a detailed analysis of microstructure evolution of TWIP steels under impact loading that establishes both the temperature and chemical composition dependencies has been reported only recently [114]: Bal et al. studied the impact response of TWIP steel samples at −170 °C, room temperature (RT) and 200 °C under Charpy impact loading in the presence of in-situ thermal imaging. The microstructure and deformation mechanisms of the as-is and deformed materials were investigated by optical microscopy, stereographic microscopy, scanning electron microscopy (SEM) and transmission electron microscopy (TEM). The findings of this study [114] demonstrated that the deformation of TWIP steel is dictated by two major twin systems at elevated temperatures, while nano-twin formation within one primary twin system dominates at low temperatures (Fig. 13). The presence and the role of nano-twins forming within primary twins were supported by the findings of Gumus et al. [115] and Bal et al. [102]. TWIP steel samples subjected to high velocity loading on a Split-Hopkinson bar setup [115] and falling hammer tests [102] exhibited nano-twins that formed within primary twins, which generated a ladder-like structure that increases the load bearing capacity of these alloys especially at low temperatures. These results are also consistent with findings from other groups such as Chen et al. [159].

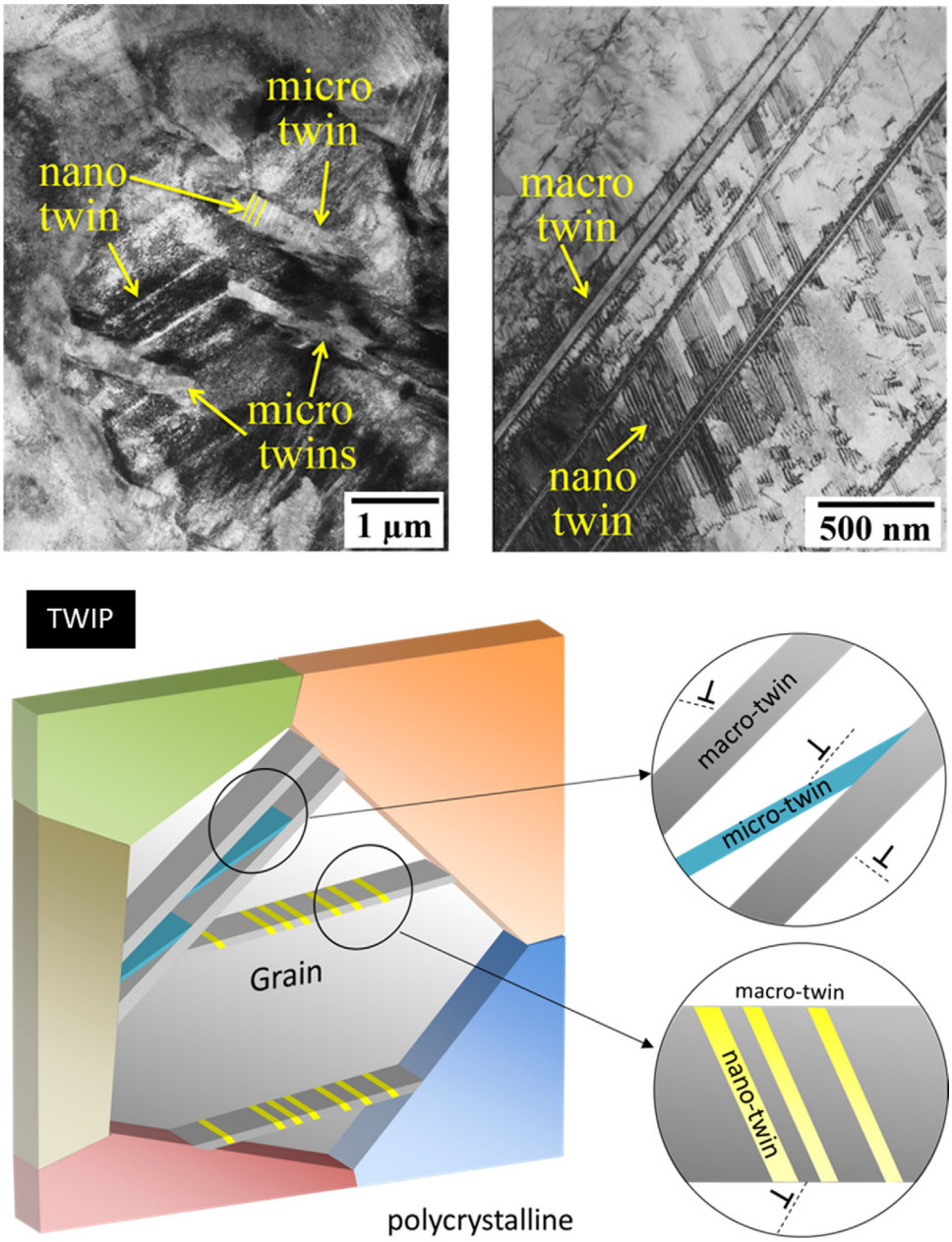

Fig. 13. (Top right) TEM images of [216]-oriented single crystalline TWIP steel exhibiting two different nano-twin variants; (top left) polycrystalline XIP steel exhibiting micro- and nano-twin interactions. (Bottom) Schematic representation of scale-variant twinning activity, and dislocation-twin and dislocation-grain boundary interactions in single- and polycrystalline TWIP steel samples.

3.3. Modeling efforts: crystal plasticity

Crystal plasticity based models have remained important conduits for exploring the TWIP properties from the microstructural standpoint [178]. Experimental studies revealed that a significant fraction of twins are on the order of nanometers, especially during the early stages of deformation [179–181]. For instance, Idrissi et al. [36] presented experimental evidence for slip-twin interactions utilizing detailed in-situ transmission electron microscopy (TEM). However, the examined area in a typical TEM sample is very limited and the obtained information is two dimensional, reflecting only the deformed surface but not the bulk texture. Thus, different methods have been employed to enlarge the inspected area as compared to a standard TEM sample: for instance, Steinmetz et al. [182] used electron channeling contrast imaging (ECCI) on TWIP steel. Based on the corresponding experimental observations, they proposed a constitutive model to simulate work hardening of TWIP steel, incorporating twin nucleation, slip-twin interactions, twin growth and temperature effect without considering any grain orientation or reorientation [182]. However, despite the considerably larger examination area of a typical ECCI sample, this technique was not able to detect the nano-twin structures that formed in the early stages of deformation due to inadequate resolution and scale difference. Moreover, nano-twins forming in the early stages of deformation evolve to macro-twins by twin boundary growth with proceeding deformation, which become visible through even confocal microscopy during later stages of the deformation, therefore are too large to be properly investigated under TEM [114]. Accordingly, the influence of mechanical twinning on the deformation response becomes more evident concomitant with increasing degree of deformation, however; in-situ and post-experimental electron-optical techniques have so far proven insufficient for drawing solid conclusions on individual contributions of slip and twinning due to the scale variation of twins throughout the plastic deformation regime.

To overcome this scale transition difficulty, various studies adopted combined experimental-numerical techniques, or fully theoretical models to understand the role of twinning in TWIP steels [29,110,162,183,184]. Allain et al. [162] developed a constitutive law for predicting the evolution of twin volume fraction of TWIP steels, and mathematically formulated the thickening of hundred-nanometer-wide micro-twin stacks into a few tens of micrometers. A different approach, where a self-consistent elastic-viscoplastic crystal plasticity approach based on homogenization of representative volume elements was utilized, theoretically demonstrated that the slip-twin interactions dictate the work hardening response in TWIP steels following about 15% strain [29]. In addition, Dancette et al. [110] investigated hardening behavior and texture development of polycrystalline TWIP steels making use of crystal plasticity-based finite element method (CPFEM) [185–187] [11–13] and statistical Taylor-type homogenization-based multisite advanced Lamel (ALAMEL) [188] method. The ALAMEL model proved successful for early stages of plastic deformation, while CPFEM approach provided more accurate predictions in the later stages of deformation, and thus, neither model was sufficient in predicting the complete deformation regime [110].

In order to successfully predict the macroscopic response behavior of TWIP steels throughout the entire range of deformation by accounting for their microscopic deformation mechanisms and textures, the well-known visco-plastic self-consistent (VPSC) crystal plasticity algorithm [189,190] developed by Lebensohn and Tome was utilized by several researchers [183,184]. For instance, Prakash et al. [183] utilized the predominant twin reorientation (PTR) method [191] adopted in VPSC to predict the twinning activity and texture evolution in TWIP steels, and compared this approach to that proposed by Kalidindi et al. [192,193]. In the PTR method, number of grains in the polycrystalline aggregate does not change, however; each grain is reoriented when the twinning volume fraction exceeds a threshold value. In Kalidindi's model, on the other hand, subdivision of grains by twinning is allowed for, and only the twinned region is reoriented rather than the whole grain. It was concluded that PTR is a better method to predict TWIP steel deformation response. Supporting evidence was forwarded by Saleh et al. [184] who investigated three different micro-deformation models utilizing VPSC: activation of only partial slip, PTR method, and twinning treated as directional slip. A comparison of these three models also revealed that the PTR method provided the best predictions of mechanical response and texture evolution, as evidenced by experimental deformation, XRD (X-ray diffraction) and EBSD results.

3.4. Case study: incorporation of slip-twin interactions on the deformation response of TWIP steels into crystal plasticity

Recently, a new crystal plasticity approach focusing on identifying and modeling the individual and collective roles of active micro-deformation mechanisms on the strain hardening response of TWIP steels was forwarded [194]. Specifically, the influences of slip, twinning, slip-grain boundary and slip-twin interactions on the deformation response of single- and polycrystalline TWIP steels were studied within the VPSC crystal plasticity framework (Fig. 14). A physics-based constitutive law was proposed and incorporated into VPSC model to geometrically

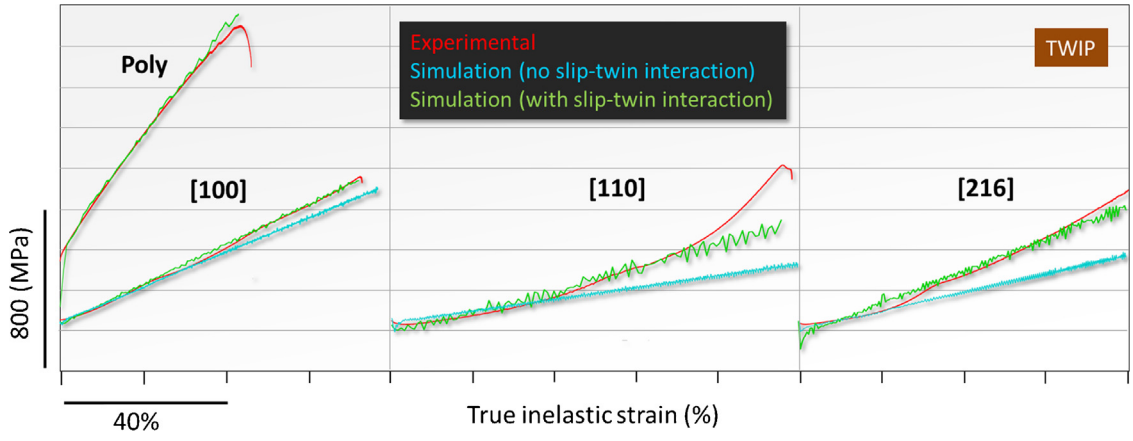

Fig. 14. Experimental uniaxial tensile deformation responses of single- and polycrystalline TWIP steel samples and the corresponding crystal plasticity simulations.

account for twin-slip interactions, where twins were modeled as effective barriers against dislocation motion. A comparison of experimental results and numerical simulations revealed that mechanical twins significantly contribute to the rapid strain hardening of TWIP steel (Fig. 14). Secondary twinning is allowed in VPSC simulations to simulate nano-twin formation within twinned regions, which is experimentally observed to be an important mechanism responsible for the superior ductility of this material.

3.5. TWIP steels: the first step towards next-generation steels

Studies to improve the quality and performance of steels date back to more than a century ago, and we have been witnessing continuous advances in steel research despite the tremendous amount of scientific and industrial work carried out in this field. Within the last few decades, many researchers focused on developing alternative materials, which actually resulted in important advances in the field of light-weight alloys. Despite these positive developments, many researchers agree that steel cannot be abandoned due its excellent formability, unprecedented strength and work hardening capacity, and the abundance of Fe on earth, even though steels possess considerably high density.

The relatively recent discovery of TWIP steels with high specific strength has reinstated steel research since then, and opened a venue towards manufacturing lighter steel components. Specifically, the twin-dominated microstructure evolution of TWIP steels paves the way for superior mechanical properties, such as improved ductility or load bearing capacity under high-velocity loading: for instance, dense twinning activity, and therefore the corresponding sub-grain cell structure formation and nano-twin formation within micro-twins lead to improved fatigue response [168] and impact toughness [114], respectively. Our current level of understanding of the deformation response of TWIP steels, along with the knowledge contributed by works that focused on Hadfield steels, will soon be leading us towards the design of superior classes of steels that are even lighter and more damage tolerant. For instance, in a very recent study by Koyama et al. [195], based on their experience with the TWIP steel microstructure, the researchers designed the microstructure of a hierarchically structured multi-phase steel by mimicking the structure of human bone, such that the active micro-deformation mechanisms successfully stopped crack propagation. Such innovative studies are expected to follow in the near future, further improving the unprecedented mechanical properties of structural steels, paving the way towards the next-generation superior steels.

In addition to mechanical and microstructural characterizations as well as phenomenological modeling, there are several rising trends in the research, particularly in the computational realms, which could readily benefit the enhancement of TWIP properties. For instance, various atomistic simulation based models (e.g. density functional theory, molecular dynamics) are becoming increasingly popular in unraveling discrete lattice scale properties [196–200]. These methods concern phenomena at the ultra-small lengthscale (nanometers to angstrom level). At the smallest lengthscale, first principles based studies are being used to predict stacking fault energy levels subjected to varying composition, lattice type etc. We have seen from experiments that composition plays a major role in dictating the inherent deformation mechanism and hence the mechanical attributes. These ab-initio predictions can serve as insightful educated bases for reducing trial-and-error based optimizations in formulating novel alloys. We will discuss specific case studies at the end of this article in this regard with more details. Similarly, there exist considerable potential for investigating the dynamic nature of deformation twinning and slip and how they relate to constitutive responses via many-body potential based molecular dynamics [196–200].

4. Fe-Mn based shape memory alloys (SMAs)

Iron based alloys represent the backbone of structural materials. Their properties are well characterized and their performance in the long term has been established through many studies [201]. The potential realization of new iron based alloys with shape memory characteristics is relatively new and is now possible with advances in computational modeling, and experiments at micro-scale focused on transformation nucleation and migration [202]. Iron based alloys with shape memory capabilities have been proposed previously but scientific investigations incorporating atomistic modeling (as have been done for NiTi SMAs [203,204]) and mesoscale experiments and modeling have been missing. Traditionally, the developments relied on lengthy studies of producing many compositions and testing. There is one set of iron based shape memory alloys (SMAs) of the FeMnNiAl variety with capabilities of high strength, low manufacturing cost, low hysteresis, and high recoverable deformations [45]. The FeMnNiAl based SMA represents a huge opportunity for further advancement.

At this time, the fundamentals of shape memory effect (SME) and superelasticity (SE) response of these iron-based alloys have not been understood. Most exhibit shape memory but not superelasticity. Shape memory refers to forward and reverse transformation upon heating and cooling under isobaric conditions as in Fig. 15(a). The occurrence of irreversible (plastic) strain can limit the SMA's functionality as shown in Fig. 15(a). Superelasticity (rubber like behavior as shown in Fig. 15(b)) refers to forward and reverse transformation upon loading and unloading at a constant temperature. The presence of plastic flow limits the recoverability. The elevation of transformation stress with increasing temperature is proportional to the entropy change given as $d\sigma/dT = \Delta S/\varepsilon_{tr}$, where $\Delta\Sigma$ is entropy change from austenite to martensite, and ε_{tr} is transformation strain. In addition to the determination of transformation stress and transformation strain, establishing the slip stress and entropy change is fundamental to SMA development.

Early work by Sehitoglu et al. [205,206] and three other groups, in Japan [207–210], Germany [211] and Ukraine [212], have investigated the main iron based shape memory alloys. We summarize the most pertinent results on iron based SMAs above in Fig. 15(c) and (d). In Fig. 15(c), we show the stress hysteresis versus transformation (equilibrium) temperature, and in Fig. 15(d) we show the transformation strain versus the transformation temperatures. The well-known NiTi, Cu-based materials have excellent transformation strains [213]. The first set of alloys is the FeNiCoTi alloys, which showed good shape memory response but no superelastic behavior. The FeMnSi alloys exhibit similar characteristics to FeNiCoTi. Both fell short of the well-known SMA NiTi with its superior traits. The development of FeMnSi alloys has been intriguing but they do not exhibit superelasticity and have huge thermal hysteresis [214,215]. The FeNiCoAlTa exhibit good SME and SE but suffer from low slip strength [210,216]. Most recently, it is the development of the FeMnNiAl alloys [45,217,218] that has invigorated renewed interest because they exhibit huge potential with strains approaching 10% exhibiting both superelastic and shape memory response. The transformation (equilibrium) temperature of FeMnNiAl is at room temperature, which can open many new applications. This is unlike the FeNiCoTa alloys and other Fe-based SMAs where the transformation temperatures are well below room temperature limiting their use. In the following section, we discuss these materials on a case-by-case basis.

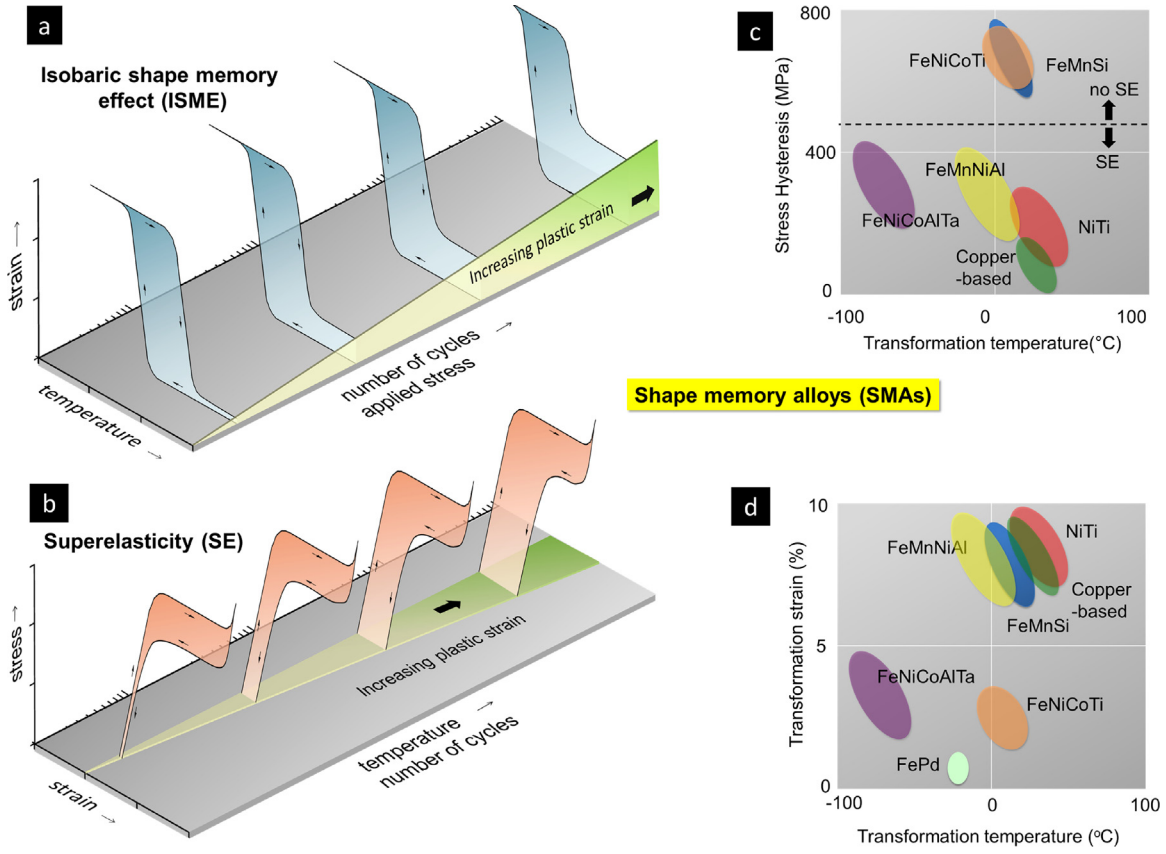

Fig. 15. (a) Schematic Illustration of Isobaric Shape Memory Effect, (b) Superelasticity in SMAs, the role of dislocation slip (plastic strain) on the functionality of the SMA are shown, (c) the stress hysteresis versus transformation temperature. The alloy FeMnNiAl exhibits superelasticity at transformation temperatures above 0 °C similar to NiTi and Cu-based alloys. The stress hysteresis in FeNiCoTi and FeMnSi is too high to induce superelasticity, and (d) transformation strain versus the Transformation Temperature. The iron based alloys are compared to two well-known SMA systems the (NiTi and Cu-based alloys). The comparison shows that FeMnNiAl (marked with a dashed line) has excellent potential.

4.1. Case study: Fe-Mn-Si and Fe-Mn-Si-Cr-Ni alloys

4.1.1. Deformation responses

The major advantages of the Fe-Mn based SMAs are their higher stiffness and potentially higher strength compared to Ni- based SMAs and lower cost and familiar processing routes already well known in steels. We review the early FeMnSi based alloys that exhibit shape memory but not superelastic behavior because of large stress (thermal) hysteresis. Then, we focus our attention on the new FeMnNiAl alloys that exhibit excellent superelastic behavior [45,217–219]. An important set of works has been undertaken by Sade and coworkers [220], who showed the sensitivity of the transformation temperatures to Mn content (Fig. 16). These results are revisted below from the work of Sade and other researchers that summarizes the role of Mn content and the magnetic transition effects on the results [45,217–220].

Earlier, Sato and co-workers [41,42,221,222] contributed to the development of Fe-Mn-Si SMAs and extensively studied their functionalities. The importance of this class of SMAs lies at their relatively low costs compared to other SMAs. It is noted in the literature [223] that the single-phase solid solution of Fe-Mn-Si alloys are the most economic SMAs although with highest recovery strain around 3%. A dramatic increase in the recovery strain (>7.5%) could be achieved at even lower cost as a result of annealing (which reduces interface density).

Composition-wise, it has been reported earlier that the alloys possessing 28–32 wt% Mn and 4–7 wt% Si demonstrate good shape memory effects [41]. The addition of chromium (Cr) increases the corrosion resistance in Fe-Mn-Si based SMAs [224]. Contrary to other better-known SMAs (e.g. Ni-Ti based), these materials have no ordered lattice. The deformation recovery properties are attributed to reversible transformation between austenitic fcc (γ) and martensitic hcp (ε) lattices. Fig. 17 presents a TEM micrograph of extended stacking faults formed as a result of deformation [225]. It is noteworthy that the martensite domains (thermally induced) are obstructed at the grain boundaries. The

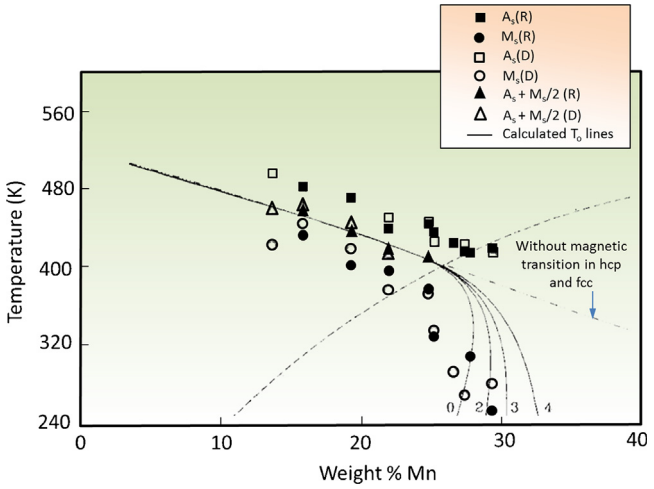

Fig. 16. The composition dependence of the transformation temperature on Mn in Fe-Mn alloys [220].

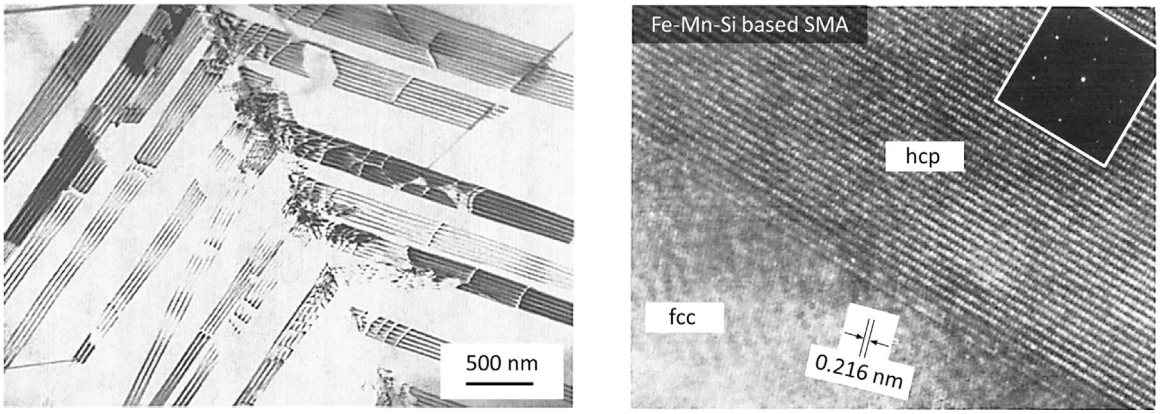

Fig. 17. Stacking faults in the deformed microstructure of Fe-Mn-Si based SMA [225]; (right) high resolution TEM evidence of hcp stacking [226].

right inset provides an example micrograph (high resolution transmission electron microscopy) showing stress-induced martensite consisting of parallel stacking faults of hcp lattice type [226]. Evidence of hcp ε phase bands can be seen in the right inset at a lower magnification.

It is confirmed from exhaustive sets of microstructure characterization that phase transformation of Fe-Mn-Si SMAs is governed by the back-and-forth glissile motions of Shockley partial dislocations [41,225]. One of the important metrics, which represents the ease of strain recovery of deformation, is the frictional stress against slipping during the reverse flow. In addition, Drucker et al. [227] studied the texture effects as a function of fabrication process. They reported the difficulties of martensitic transformation with respect to different grain orientations and reduced grain sizes. Kajiwara and co-workers [228–230] suggested that the pre-existent stacking faults can facilitate fcc-to-hcp forward transformation.

4.1.2. Slip- assisted fcc ↔ hcp phase transformation and other considerations

Fig. 18 illustrates the fcc-to-hcp transformation. The process is best understood in the form of gliding of multiple Shockley partials of $^{1}/_{6}\langle 112\rangle_{fcc}$ type on alternate $\{111\}_{fcc}$ planes. In the lower right schematic, the hcp stacking (ABABABAB$\cdots$) of $\{111\}_{fcc}$ planes is created once the glissile partials have swept the region. In the top inset, one can see that the motion of the Shockley partial causes the re-positioning of atoms on that plane so that an hcp staking is created. The positions of atoms in the immediately adjacent layers i.e. in the un-slipped ones remained unchanged. With continued deformation of the material, the volume fraction of alternate slipped and un-slipped planes are increased, thereby giving rise to the hcp martensite domain. It should be noted that the motion of a single Shockley partial creates a plane of stacking fault in its wake. Thus, the slip-assisted transformation (fcc-to-hcp lattice) can be

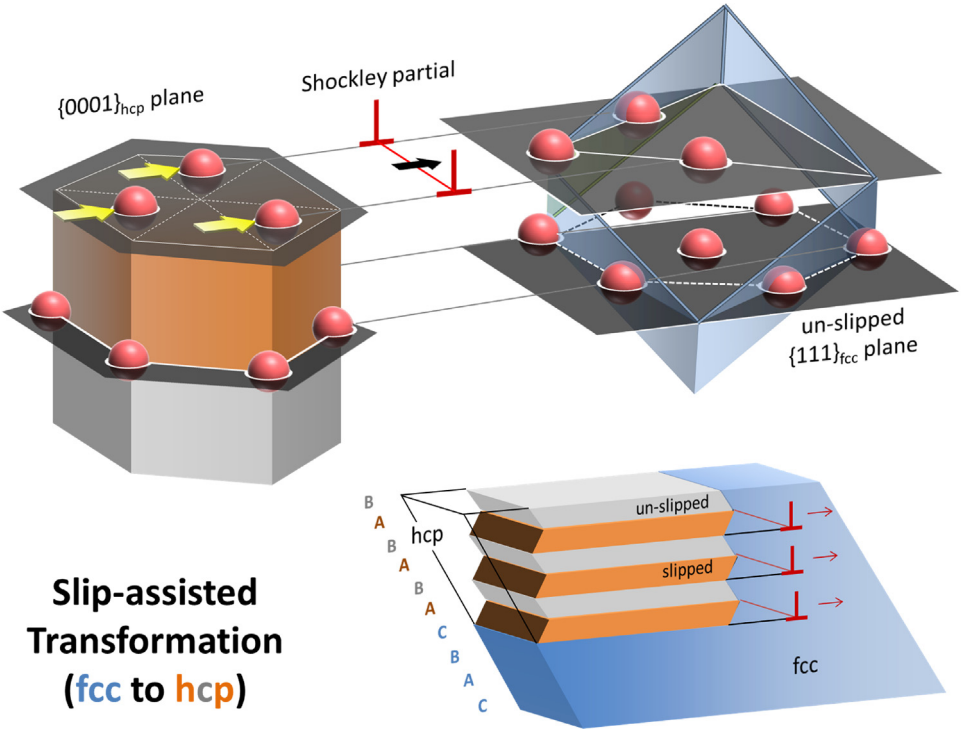

Fig. 18. Schematic illustration of fcc-to-hcp transformation mechanism as assisted by dislocation glide.

associated with low intrinsic stacking fault energy [231,232]; however, results contrary to this idea exists [233,234]. Another consequence of low stacking fault energy is the propensity to nano-sized twins in the microstructure [235]. Interestingly, Wen et al. [223] reported that the suppression of annealing twins can lead to an enhanced strain recovery attributes in this material. They asserted that a reduced density of twin boundaries in the polycrystalline microstructure contributes to a greater degree of transformation reversibility.

An understanding of dislocation mechanics can open up interesting avenues of research. For instance, the atomistic energy landscape for partial slipping is well established in conventional fcc materials. The utilities of these energies in conjunction with Peierls-Nabarro concepts [236] have also been examined in recent years. The lattice resistance arising from atomic shear is overcome by applied stresses. The long-range elastic fields of slip and short-range core effects would play a significant role in dictating the inherent resistance to transformation. With rapidly emerging literature in the computational materials science [237,238], it remains to be seen how similar analysis will cast more light into Fe-Mn-Si based SMA behaviors.

4.2. Case study: Fe-Mn-Ni-Al alloys

4.2.1. Thermomechanical properties and microstructure

Fe-Mn-Ni-Al alloys [45–47] have drawn considerable attention due to their superior pseudoelastic traits. Transformation strains (upwards of 8%) are reported at the room temperature along with a low hysteresis. Moreover, the transformation stress is observed to be nearly independent of temperature over a broad range starting at −196 °C to 240 °C. A Clausius-Clapeyron slope (i.e. $\partial\sigma/\partial T$) of 0.53 MPa/°C has been reported by Tseng et al. [239]. This value is significantly small in comparison with that of a more conventional SMA such as NiTi, which is characterized by $\partial\sigma/\partial T$ = 6–8 MPa/°C [240]. The attribute of having insignificant temperature dependence over a wide temperature window holds considerable promise for industrial applications. The required functional temperature for different industries (e.g. aerospace, automotive, seismic) varies significantly. The broad operating window for superelasticity along with low costs of the constituent elements makes the Fe-Mn-Ni-Al alloys particularly attractive SMAs.

In addition, these alloys offer further property enhancement through suitable thermo-mechanical treatments. For instance, Tseng et al. [46] subjected single crystals to an aging treatment of 200 °C for 3 h, which reportedly resulted in nano-sized (6–10 nm) precipitates (enriched in Ni and Al). In their study, (Fig. 19), the presence of nano-precipitates is substantiated using different characterization techniques. On the left, high resolution TEM image of the B2 precipitated lattice is marked with a dotted line. The right figure represents a three-dimensional reconstruction of the precipitates (in terms of Ni- and Fe-rich regions) in the heat-treated microstructure using atom probe tomography. The precipitates affect the deformation tendency by influencing plastic flow and transformation behavior. Smaller precipitates offer less resistance to plastic flow, thereby increasing the dissipation energy (i.e. corresponding to large hysteresis). On the other hand, large precipitates constitute more effective barriers to plastic deformation, thus promoting phase transformation, which in turn is manifested in smaller hysteresis. In addition, Niendorf and colleagues developed a thermal treatment technique to grow bamboo crystals in the FeNiMnAl alloys and the results are shown in Fig. 20 [217]. The results are far more encouraging than previous Fe based SMAs where the strains and superelasticity were rather limited [205,206]. Quite interestingly, the underlying deformation mechanism of phase transformation in this class of SMAs is governed by a reversible transformation between bcc ↔ fcc phases assisted by dislocation motions (discussed next).

4.2.2. Slip-assisted bcc ↔ fcc transformation

The presence of massive dislocation activities during the phase transformation has been confirmed through electron microscopy. The fundamental mechanism by which atoms are repositioned during bcc ↔ fcc conversion was first addressed by Bogers and Burgers [241,242]. Subsequently, Olson and Cohen [243,244] incorporated the roles of glissile partial dislocations, and established their association with the transformative displacements of atoms. The entire mechanism is illustrated in Fig. 21. In essence, the process is characterized by simultaneous shear of two different systems – $\{110\}\langle 110\rangle_{bcc}$ and $\{111\}\left\langle 112\right\rangle_{fcc}$. When a dislocation of $1/8\langle 110\rangle_{bcc}$ type on the $\{110\}_{bcc}$ plane glides on every alternate parallel plane, however, along opposite directions, the atoms swept by the dislocation are relocated to form fcc lattice. Similarly, the passage of a partial dislocation of type $^1/_6\left\langle 112\right\rangle_{fcc}$ on every third $\{111\}_{fcc}$ plane (which is parallel to the $\{011\}_{bcc}$ planes) would displace in-plane atoms to fcc positions. It should be noted that the motions of partial dislocations create stacking faults in their wake. In the foregoing process, a fully formed fcc lattice would be created when the stacking faults from two different straining systems (assisted by dislocation glide) would intersect. The transformation stress for FeMnNiAl alloy, utilizing the double

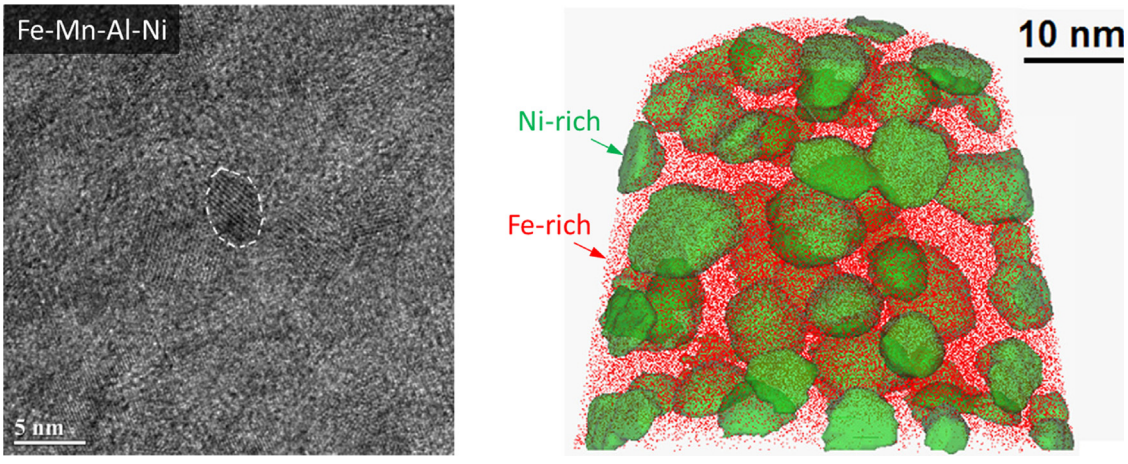

Fig. 19. (a) High resolution TEM image of B2 precipitate in Fe-Mn-Al-Ni SMAs, and (b) 3D rendition of the precipitates using atom probe tomography [46].

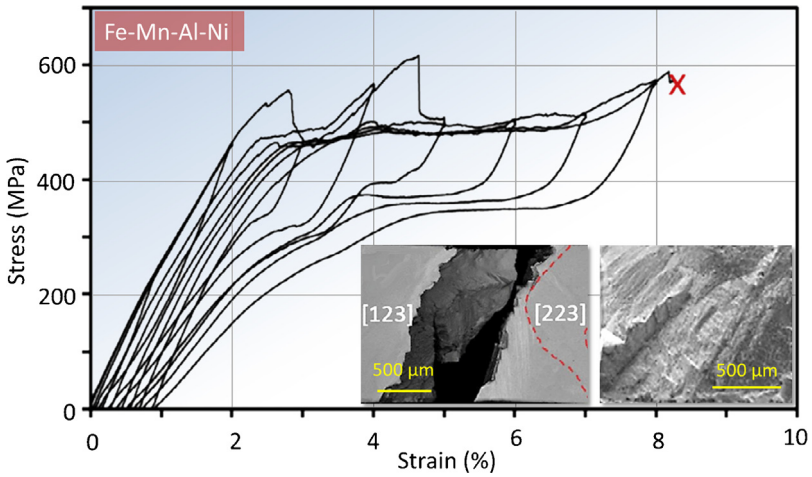

Fig. 20. The superelastic response of FeNiMnAl alloys displaying large recoverable strain [217]. The results are obtained on bamboo crystals and show the considerable promise of these classes of SMAs.

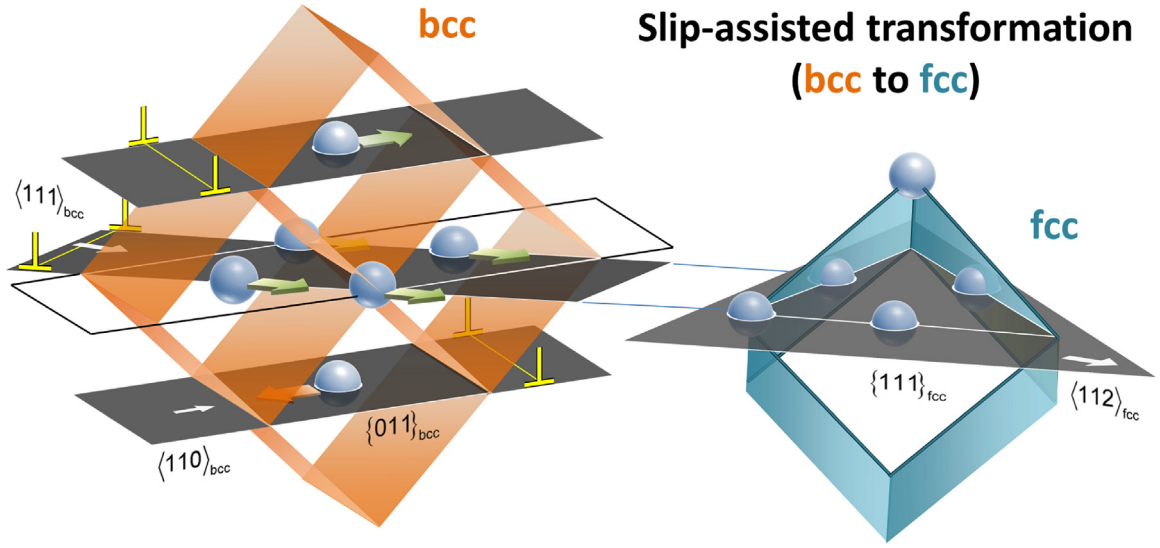

Fig. 21. Schematic illustration of bcc-to-fcc transformation mechanism as assisted by dislocation gliding on parallel planes (see text for details).

shear mechanism has been calculated recently, which is in agreement with experiments [40].

5. Fe-Mn based high entropy alloys (HEA)

5.1. Structure-property correlation in CoCrFeMnNi HEAs

5.1.1. Engineering of microstructure properties

The high entropy alloys reported in the literature consist of constituent elements, which are of fcc, bcc and hcp lattice structures [60]. Interestingly, the existing research suggests that the crystal structure of HEAs is either of fcc or bcc symmetry [245]. It has been generally known that some chemical species are fcc stabilizer (e.g. Ni, Co, Mn) while other elements of refractory types stabilize the bcc phase (e.g. Cr, Fe). However for the multi-element HEAs, a complex interplay involving the volumetric ratio of atoms and electronegativity of individual constituent species would dictate the final structure [246]. The mixing of diverse transition metals also has the effect of dramatically lowering the stacking fault energy (SFE) of the alloy. In Fig. 22(a), the SFE of materials ranging from pure Ni to equiatomic multi-component alloys are presented after Zaddach et al. [247]. It follows that the SFE is reduced with increasing number of chemical species when alloyed equiatomically. The data are collected from experimental measurement as well as first principle based calculations. It is noteworthy that with the addition of elements the rate of decline in the SFE level becomes somewhat saturated. This observation implies that simply adding more transition metals may not lead to further reduction in the SFE. A comparison is made among the materials reportedly having the lowest levels of SFE in Fig. 22(a). The alloy designated "best HEA" has the following chemical formula: $Ni_{14}Fe_{20}Cr_{26}Co_{20}Mn_{20}$ having the lowest SFE (less than 4 mJm^{-2}). These results bear important implications for the plastic deformation mechanism in HEAs.

In the context of conventional materials, a low magnitude of SFE has earlier been associated with enhanced twining propensity [248–251]. The reason is that a low stacking fault energy makes possible the formation of wide stacking faults i.e. partial dislocations connected by fault planes. The result is less cross-slipping with a prevalence of planar slip morphology. Moreover, the nucleation of extended dislocations is strongly correlated with the twinning. Indeed, as we will discuss next, the deformation micromechanism of the HEAs is characterized by widespread twinning along with dislocation-mediated plasticity. The

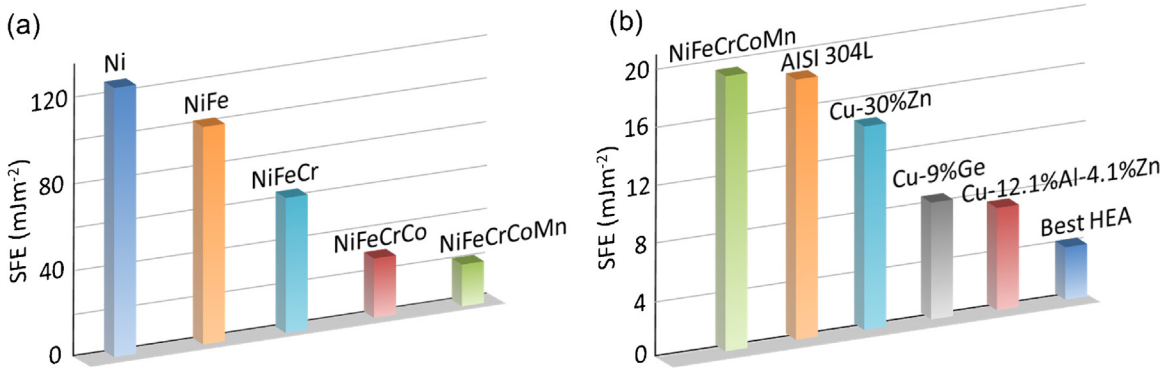

Fig. 22. (a) A comparison of stacking fault energy (SFE) of various materials, and (b) SFEs of various alloys [247].

outcomes of such microscopic processes are remarkable, in that a considerable toughening attribute results therefrom on the macroscale.

5.1.2. Observed deformation behavior

The particular example of CoCrFeMnNi alloy presents a case with high configurational entropy and a stable microstructure consisting of a single phase solid solution [7]. This material is known to undergo a simultaneous increase in strength and ductility when the temperature is lowered from room temperature (293 K) to the cryogenic state (77 K) [49]. This trend is very unusual in that strength and ductility maintain an inverse proportionality in most conventional metallic alloys. The underlying reason for a concurrent enhancement of elongation and strength in CoCrFeMnNi HEAs has been related with a deformation mechanism mediated by both dislocation slip and twinning [116] at 77 K. The occurrence of twinning is facilitated by the low stacking fault energy (20–25 mJm^{-2}) of the alloys [247,252]. By contrast, dislocation based plasticity has been observed as the primary deformation mechanism at room temperature. In addition, HEAs possess high fracture toughness in comparison with other metallic materials such as low-alloy stainless steels [8,253,254].

In the inset of Fig. 23, the true stress versus strain at 293 K and 77 K are compared (after Laplanche et al. [255]). The increase in both strength and ductility at 77 is noteworthy, a trend consistent with other literature reports as well [8,49,116,256]. A TEM study of the deformed microstructure at different strain levels then revealed the mechanism of the strengthening and microscopic strain accommodation at 77 K. At the early stage of deformation (strain, $\varepsilon = 2.1\%$), the presence of planar dislocations from several slip systems are noted piled up against grain boundaries. Occurrence of nanotwins (5–20 nm) in few grains is first observed at $\varepsilon = 6\%$ while the majority of the grains still demonstrating prevalence of slip. With increasing strain, twinning becomes the primary mode of plastic deformation, the evidence of which is also quantified in terms of the twin volume fraction. It is interesting to note that the later stage of deformation involves newly nucleated twins with more finely spaced distribution. From Fig. 23, the mean twin spacing versus true strain as measured by Laplanche et al. indicates a saturation stage. These experimental results establish

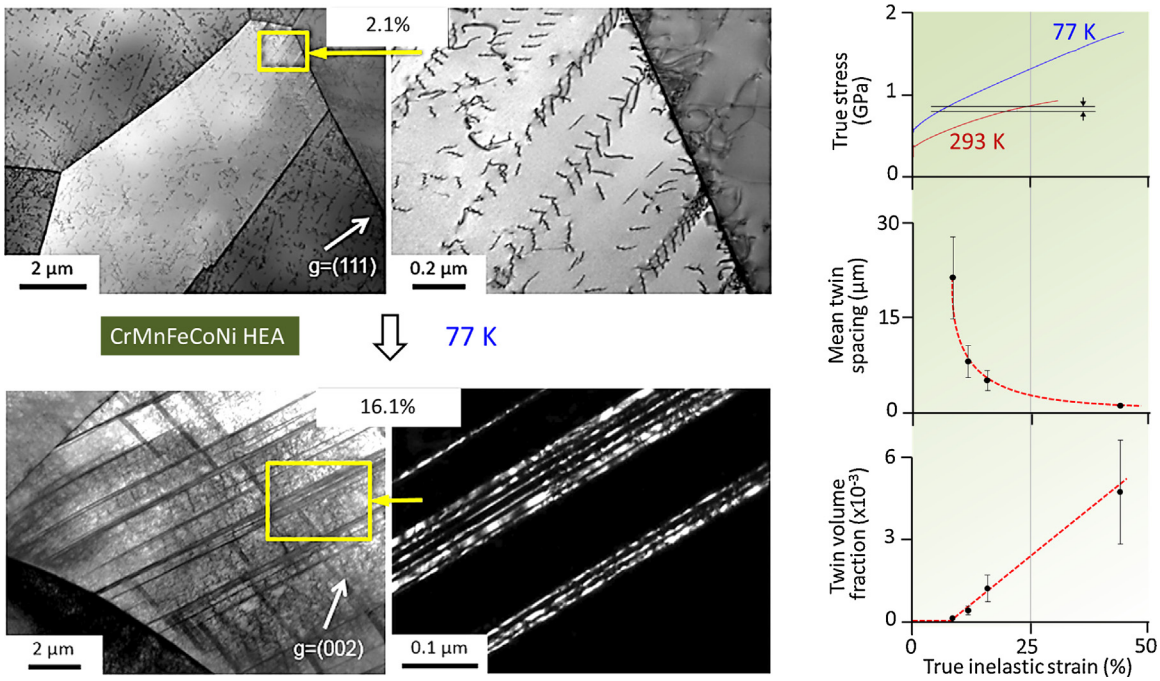

Fig. 23. (Right) Plastic stress-strain responses at liquid nitrogen temperature (77 K) and 293 K along with variation of twin dimension and volume fraction with increasing strain (Left) TEM micrographs at different strain (global) levels showing the evolution of the plastic deformation mechanism from slip- to twinning-mediated ones [255].

that the origin of the superior strength and ductility is related with pervasive twinning accompanied by slip at cryogenic temperature (77 K). The underlying rationale is discussed next.

5.1.3. A rationale for constitutive responses

In the context of conventional materials, the strengthening effects during plastic deformation originate from dislocation obstruction due to interfacial defects [257,258] as described by the classical Hall-Petch relationship [259,260]. If the density of grain boundaries is high, the material undergoes an increased degree of flow stress, however, at the significant expense of ductility. Quite interestingly, a high volume fraction of twin boundaries have been associated with augmented hardening attributes with the retention of considerable ductility [248,261]. Recall that the inelastic deformation CoCrFeMnNi alloys (at 77 K) is initially mediated by dislocation activities and twinning ensues at more advanced stages (beyond 6% strain). The formation of twins essentially leads to further interfacial density in addition to the existing grain boundaries within each host grain, giving rise to enhanced dislocation obstruction. Consequently, the flow stress is increased. Now, the question remains as to what underlies the enhanced ductility. Unlike any other grain boundaries, a coherent twin boundary possesses the distinctive ability to allow glissile dislocation motions along the interface [262–265]. As a result, considerable plastic straining can be achieved when incident dislocations, as impinging on the newly forming twin boundaries, continue to glide and contribute to twin migration.

The foregoing deformation scenario is schematically illustrated in Fig. 24. These mechanistic implications, albeit discovered in conventional alloys, are useful in rationalizing the enhancement of low temperature strength and ductility of CoCrFeMnNi HEAs. It should also be noted that the single phase solid solution of the CoCrFeMnNi HEA possesses a low stacking fault energy, which is known to give rise to the splitting of a full dislocation into a Shockley partial pair in fcc crystals [247,252]. The increased propensity of partial slip due to low stacking fault energy has earlier been regarded as a precursor to deformation twinning [66,248]. It poses an interesting avenue of future research to investigate the role of solute atoms giving rise to different magnitudes of fault energetics. Such findings will bear important implications for manipulating resistance against slip and/or twinning. For instance, the partial dislocations in the HEA lattice glide through an environment of randomly distributed atoms, the nature of which would vary substantially from one location in the lattice to another. The situation is depicted in Fig. 24. It is worth recalling that the stacking fault energy landscape could be a function of the positioning of individual solute atoms. This is essentially a problem that could most appropriately be addressed through ever-emerging atomistic simulations tools such as density functional theory, molecular dynamics [266,267].

5.2. Temperature-dependent deformation response

The remarkable cryogenic properties of CoCrFeMnNi HEAs motivated considerable number of investigations on the issue of temperature dependence. For instance, George, Otto, Eggeler and co-workers [53,116] reported its stress-strain responses as well as deformed microstructure for a wide temperature spectrum (from 77 K to 1073 K). The measured stress-strain responses, starting with initially dislocation-free microstructure (achieved via thermo-mechanical treatment) are presented in the middle inset of Fig. 25. Two sets of material with different grains sizes (4.4 μm and 155 μm) are found to follow the same temperature dependence. At the lowest temperature studied (77 K), the material exhibited highest yield, tensile strength and elongation. By contrast, the maximum test temperature of 1073 K corresponded to a degraded strength and ductility. The temperature-mechanical properties are more pronounced in the coarse-grained (155 μm) specimens. The presence of stacking faults is frequently noted at different strains and temperatures, for example, (2.4%, 2.1% and 1.7% at 77 K, 293 K and 873 K respectively) as in Fig. 25(a), (b) and (c). It is inferred that the prevalence of Shockley partial dislocations of type $1/6\langle 112\rangle$ would be bounded by these planar faults. It is worth recalling here that pervasive dissociated slip has earlier been associated with greater propensity to deformation twinning in other fcc alloys [248]. While the slip activities are the signature of earlier stage of deformation (up to 2.4%), the more advanced stages are characterized by pervasive deformation twinning. TEM analyses attest to the widespread presence of nano-sized twins as shown in Fig. 25(d), (e) and (f). Fig. 25(d) presents the evidence of densely-spaced twins transmitting (appearing as thin bands) past grain boundaries. A high resolution view as in Fig. 25(e) reveals the twin and matrix (labeled as "1" and "2" respectively). An even closer inspection is provided in Fig. 25(f) with all the twinning elements labeled i.e. $K_1 = (\bar{1}1\bar{1})$, $\eta_1 = [\bar{1}12]$, $K_2 = (\bar{1}11)$, $\eta_2 = [\bar{1}1\bar{2}]$ (twinning shear, s, being $1/\sqrt{2}$). The mirror symmetry of atoms is also clearly noticeable.

The above example represents the general findings in the literature as to the nature of deformation micromechanism of

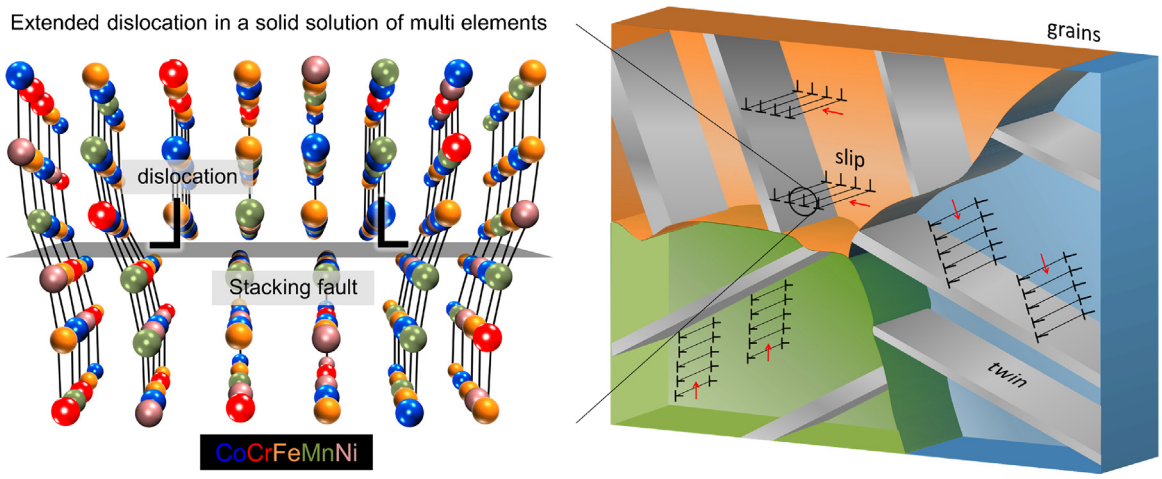

Fig. 24. (Right) Schematic illustration of the typical deformed microstructure of the HEA where concurrent twinning and slip dictate the global mechanical properties. (Left) schematic of multi-element atomic environment at a single extended dislocation lengthscale (see text for full discussion).

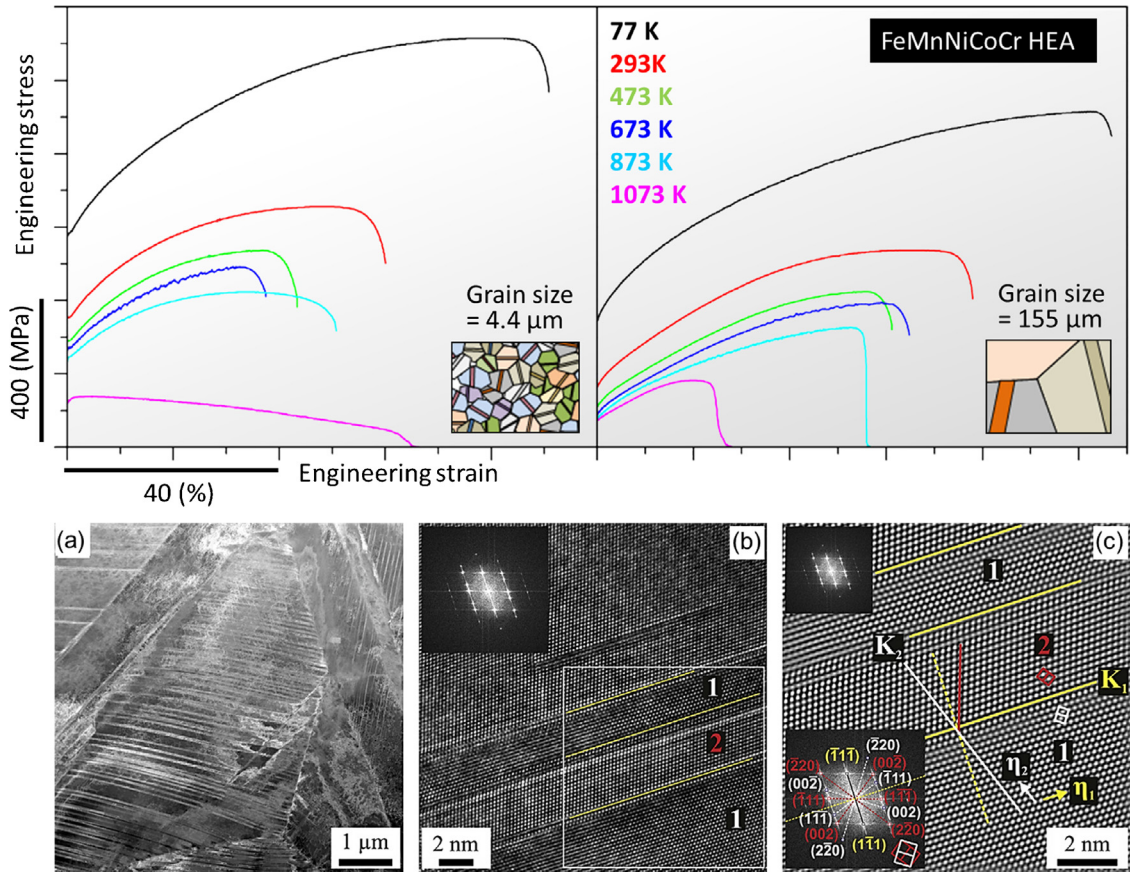

Fig. 25. (Top) plastic stress-strain responses at various temperatures for the two cases of grain sizes. (Bottom) high TEM micrographs reveal the details of twinning [116].

CoCrFeMnN HEAs. At the higher temperature (above 293 K), dislocation-mediated plasticity becomes more and more dominant. On the other hand, the lower temperature regimes are characterized by an increasing predilection of deformation twinning. It should be noted that the initiation of the twinning is temperature-independent. In other words, the critical stress for twinning is a unique quantity as noted by Laplanche et al. [255]. They determined the CRSS for twin to be 235 ± 10 MPa.

5.3. Fracture properties

The unique ability of CoCrFeMnN HEAs to transition from planar slip-mediated plasticity to nano-twinning has dramatic effects on the fracture behavior as well. Gludovatz et al. [8] noted a high fracture toughness as a direct consequence of ductile micro-void based cracking mechanism at cryogenic condition (77 K). They reported a fracture toughness magnitude as high as $200\,MPa\sqrt{m}$ for a range of yield strength (730 MPa to 1230 MPa). This value is comparable to austenitic stainless steels (whose applications are also slated for cryogenic settings [268]). The origin of such remarkable damage tolerance is traced back to twinning-dominated plasticity at low temperature.

In Fig. 26, the crack growth mechanism at room and cryogenic temperatures (293 K and 77 K respectively) are characterized [8]. The crack is initiated at the notch, and advancing therefrom. The scanning electron microscopy (SEM) images suggest that the nature of the cracking is of ductile type as dominated by micro-void coalescence. The crack path at 77 K is also notably tortuous. Electron backscatter diffraction (EBSD) in the vicinity of the lower temperature crack attests to the presence of nano-sized annealing twins. By contrast, the higher temperature crack advances by dislocation-medicated plasticity leading to pronounced grain misorientations. The deformed microstructure in the wake of the crack is characterized by dislocation cell structures, a consequence of extensive slipping. These results on the cracking of the high entropy CoCrFeMnN alloy at the cryogenic condition are consistent with other literature reports on the twining being the principal reason for superior toughness [248,269,270]. These findings motivate the development of predictive capabilities for assessing damage tolerance in presence of substantial twinning-mediated near-tip plasticity as has recently been demonstrated for the nano-twinned materials [271–274]. In particular, the concurrent presence of twins and slip has been associated with superior fatigue crack growth resistance as a result of beneficial outcomes of interfacial plasticity [275–277]. It remains to be seen how similar predictions, specifically addressing the high entropic state along with plastic mechanisms, are forwarded to further rationalize the empirical fracture behaviors in the CoCrFeMnN or in other HEAs in general.

5.4. Role of substitutional elements

With a view to experimentally assessing the feasibility of other HEAs, Otto et al. [52] investigated the effects of substituting Ni, Co, Cr and Fe elements with Cu, Ti, Mo and V. They were able to fabricate new multi-component alloys, namely, CoCrFeMnCu, TiCrFeMnNi, CoMoFeMnNi, CoVFeMnNi and CoCrVMnNi. It is worth noting that these substitutional transition atoms possess similar atomic radii and electronegativity compared to the ones being substituted. The idea was to examine whether the same configurational entropy would be retained, and the new alloys would consist of single phase. Fig. 27 shows the x-ray diffraction

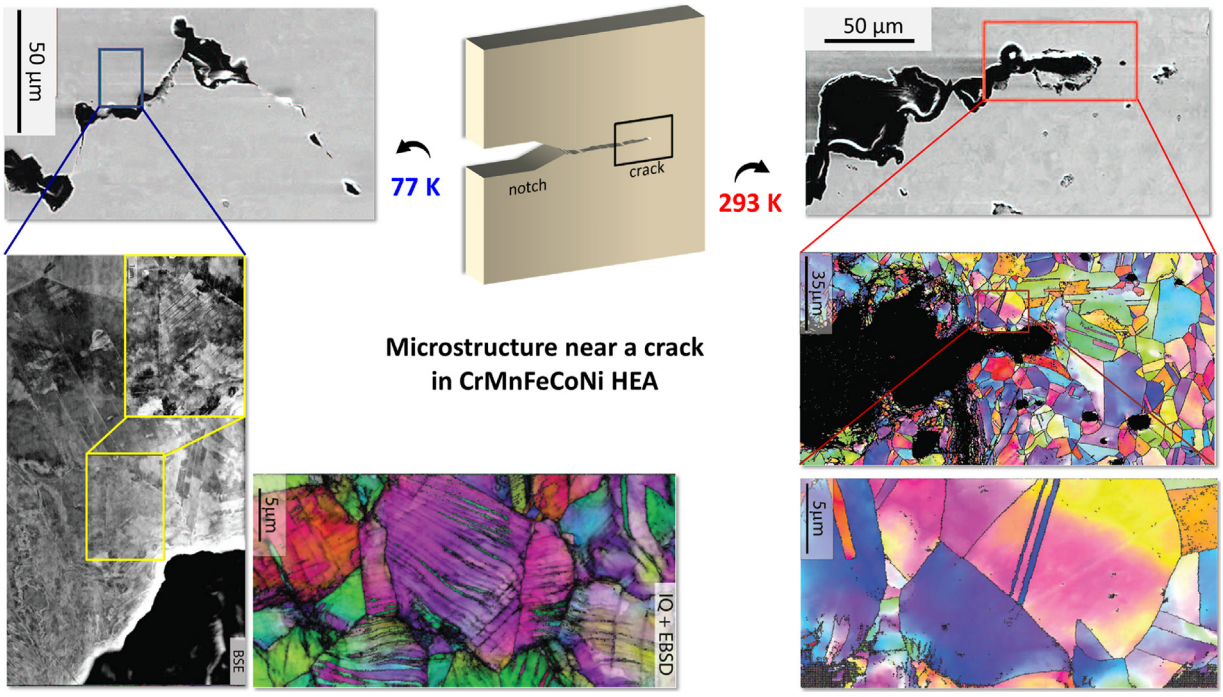

Fig. 26. Microstructure of the HEA near the crack tip at low (77 K) and room temperature. The presence of twin is evidenced through the EBSD analysis [8].

peaks along with the microstructural characteristics of these alloys [52]. As can be seen, the "base" CoCrFeMnNi alloy is characterized by large elongated grain structure, which is a result of directional solidification. The corresponding XRD peaks confirm the presence of a single fcc phase. When Ni is substituted by Cu (i.e. in CoCrFeMnCu), the existence of a dual phase (both fcc) structure is noted. For the case of Mo substitution (CoMoFeMnNi), needle-like structure is evident in the microstructure comprising fcc solid solution and μ phases (which is common for Co, Mo, Fe mixing [278]). For the HEA with Ti (TiCrFeMnNi), four different phases are noted with fcc solid solution being predominant. The CoVFeMnNi HEA possesses elongated grain structures (similar to the CoCrFeMnNi microstructure) with dispersed σ phases enriched in vanadium (V). An enhanced tendency to form σ phase is further

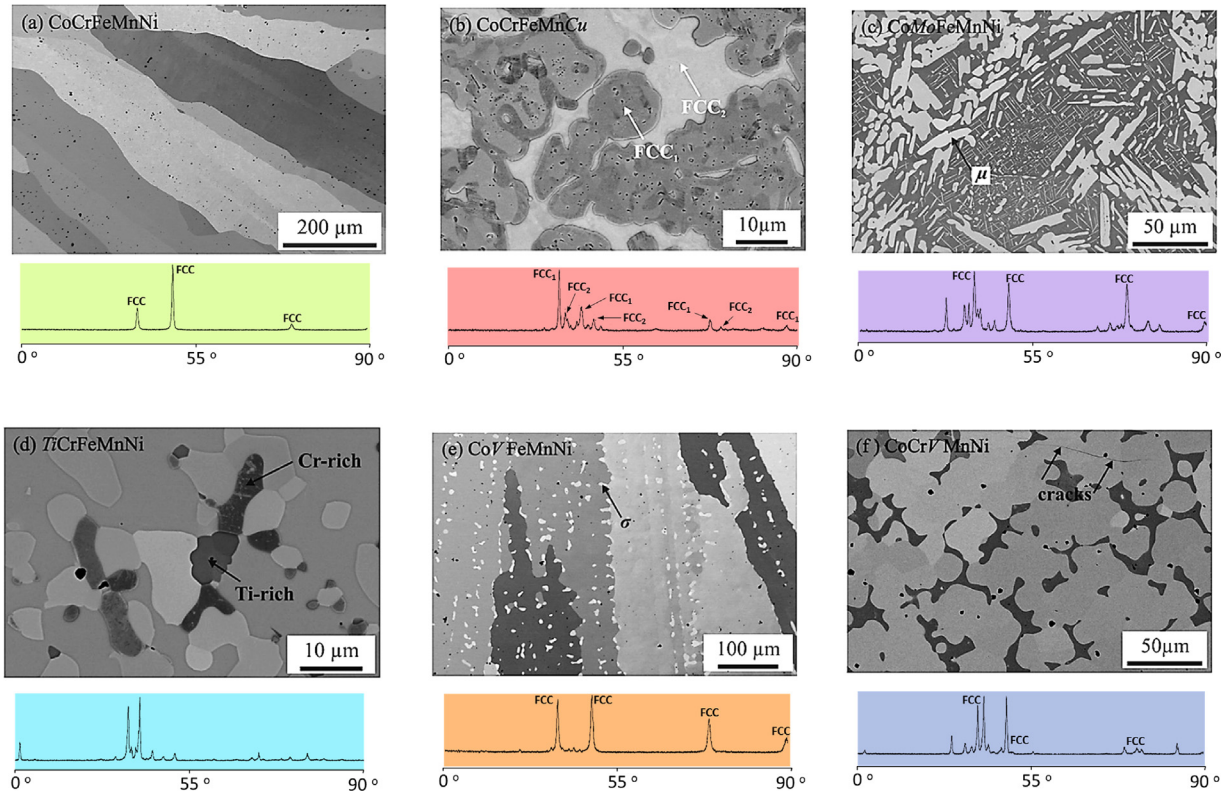

Fig. 27. Microstructure of various multi-element alloys with corresponding X-ray diffraction peaks [52].

evidenced in the CoCrVMnNi alloy, which reportedly contributes to micro-crack formation due to its brittle nature. From these careful characterizations, it is evident that the substitution with other types of transition chemical species can have dramatic consequence in phase stability. Only the CoCrFeMnNi alloy is of monophase structure while the other varieties contain multiple topologically closed-pack phases.

Otto et al. [52] also performed thermodynamic analysis, which in conjunction with the foregoing experimental observations leads to important conclusions. First, the substitutional elements (Cu, Ti, Mo and V) did not retain the same configurational entropy as the "base" CoCrFeMnNi alloy. Therefore, a single solid solution was not achieved in the new equiatomic quinary alloys. Rather, the microstructures of these new alloys are characterized by multiple phases with intermetallic compounds or two fcc solid solutions. In these substitutional alloys, a propensity to minimize the total enthalpy and entropy was noted, which is unlike the maximized configurational entropy in CoCrFeMnNi. Overall, it was inferred that the mere condition of achieving high entropy is insufficient to achieve ideal solid solution (i.e. single phase) microstructure, and can suppress the formation of secondary phases. Consequently, the strategy of only increasing the number of elements to manufacture single-phase high entropy (near ideal solid solution) alloys needs further consideration.

5.5. Future promises: predicting new multi-component solid solutions

Typically, phase diagrams are available for binary alloy systems (or at most ternary ones) from empirical observations correlating phases with constituent concentrations, temperature and pressure. Since the conventional rules of mixing (e.g. Hume-Rothery) results in multi-phase structures, ongoing efforts are directed at establishing rules for achieving a single solid solution. A single phase HEA is desired since it would possess the highest configurational entropy. Currently, the challenge of developing new HEAs is associated with not having a robust phase diagram for multiple elements that can assist in concocting a solid solution of, say, five or more chemical species [51,279–281]. Consequently, trial-and-error based empirical approaches are employed. Nonetheless, there are potential predictive capabilities, in particular, through a combination of first principles models and calculations of phase diagram (CALPHAD) [50,282]. It should be recalled here that ab initio methods are based on Schrodinger's equation while the CALPHAD methods are based on principles of thermodynamics (e.g. minimization of Gibbs free energy while maximizing entropy).

For instance, using density functional theory (DFT) simulations, Gao and Alman [50] examined atomic diffusion properties relevant in recrystallization processes of multi-component alloys. By accounting for the inherent bonding landscape, they predicted the most favorable combination of chemical species, which are most likely to form single-phase solid solution. One noteworthy finding was that the alloy compositions whose liquid state lacks short-range ordering and segregation are more likely candidates for single-phase HEAs. In addition, they utilized CALPHAD method to examine the promise of new fcc solid solutions. Zhang et al. [282] conducted extensive CALPHAD based predictions of single-phase alloy, which were in good agreement with experimentally known HEAs (e.g. CoCrFeMnNi). It remains to be seen how future alloys could be fabricated with the aid of these predictive tools.

6. Latest modeling approaches: atomistics

Due to the promises of the Fe-Mn based alloys having diversified qualities, many atomistic studies have been undertaken so as to uncover discrete lattice effects [119,120,283–288]. The question of interest involves how the addition of different alloying elements can influence the alloy attributes at the crystal level, which would eventually reverberate across multiple lengthscales to affect the macroscale properties. Below we elaborate on several case studies, insight from which elucidates many empirical behaviors in the Fe-Mn based alloys.

6.1. Ab-initio predictions on Fe-Mn based alloys

By examining the Fe-Mn system using first principles calculations, Gebhart et al. [285] found that a disordered distribution of magnetic moment underlies accurate prediction of elastic properties (compared to experiments) for the binary composition. Their calculations ruled out the possibility that Fe-Mn system possesses non-magnetic or antiferromagnetic attributes at the lattice level. In addition, Gebhardt et al. [286] computed the elastic constants for Fe-Mn-Al and Fe-Mn-Si alloys from first principles. They found that the addition of Al (up to 8 at.%) to the Fe-Mn binary system has been associated with a substantial depreciation of the shear and Young's moduli (by 20%). Similar effects are predicted for the case of Si-alloying albeit being not as dramatic (with a drop of 7% in both moduli). By modeling Fe-Mn-C alloys, Reeh et al. [287] found that the carbon addition (from 1.5 to 3 at.%) has only insignificant role in altering the moduli and lattice constants (for a Mn-content ranging from 28 to 37.5 at.% and for 60.6 to 69.8 at.% Fe concentration). The reason is attributed to the minimal effect of incorporating carbon atoms upon the electronic structure of the metallic lattice. Notice the very similar nature of electron density distribution between Fe-Mn and Fe-Mn-C alloy as in Fig. 28. These results would essentially motivate future research for fine-tuning the alloy properties based on sub-lattice descriptions.

6.2. Effect of N addition in pure Fe

As discussed in Section 2.3, the experimental results on single Hadfield steel suggest that the presence of N imparts considerable hardening attributes. By characterizing the deformed microstructure, the origin of the strengthening effects has been associated with the formation of nitride precipitates, which create enhanced obstruction to plastic flow. Interesting insight is obtained from density functional theory (DFT) regarding the role of N solutes in the pure Fe lattice. These results bear important relevance in understanding the formation of stacking faults in the N-alloyed Hadfield steel.

Kibey et al. [119] utilized the concept of generalized stacking fault energy (GSFE) surface to explore the nitrogen-induced variation in the fault energetics. The basic premise is that when two crystal blocks are sheared rigidly against each other, the atomic lattice provides resistance, which varies non-linearly and consists of peaks and valleys (Fig. 29). This could be represented by the energy differential (normalized by area) between the original lattice and the displaced one [289]. Fig. 29 shows the model concept as well as the computed GSFE surface. Kibey et al. reported two major effects on the GSFE levels, namely: (a) the concentration of N, and (b) the position of N solute with respect to the fault. They reported that for the same concentration, the positioning of N solutes father from the fault reduces the energy level. Increasing N content raises the energy level. The reduction of stacking fault energy is correlated with the widening of stacking fault planes. This finding is interesting, in that electron microscopy studies on N-alloyed Hadfield indicated presence of extended dislocations. Per the ab-initio predictions, in addition to forming nitride precipitates, the nitrogen atoms are most likely to contribute to the planar slip characteristics of these alloys. By providing an

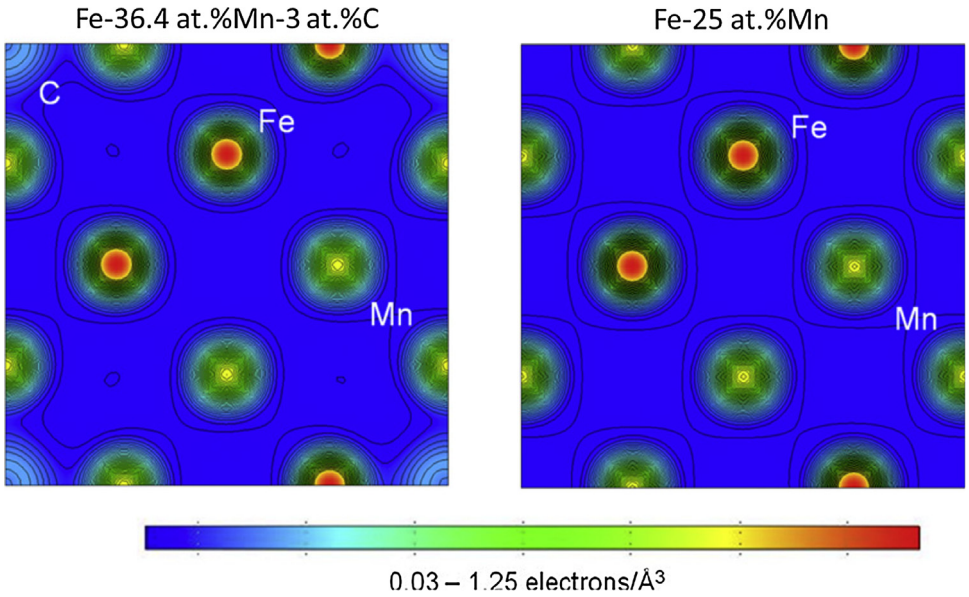

Fig. 28. Electron charge density distribution in Fe-Mn and Fe-Mn-C alloys as computed from first principles [287].

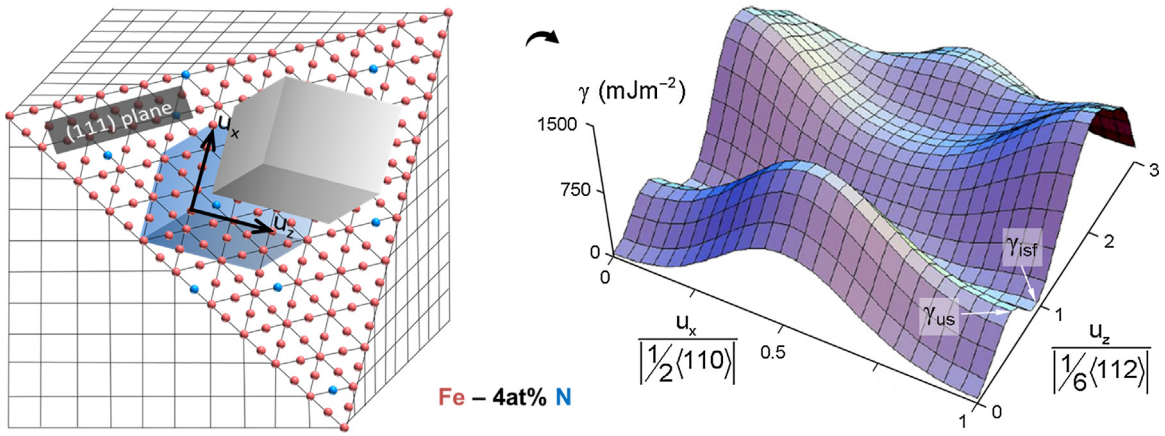

Fig. 29. Fault energy surface computed from density functional theory. Unstable stacking fault energy, γ_{us} represents energy barrier to slip while the intrinsic stacking fault energy, γ_{isf} denotes the ease of stacking fault (i.e. extended dislocation) formation [119].

energy-based rationale for observed deformation mechanism, these results call for further research in this regard.

7. Concluding remarks

This review compiles the literature on the four classes of Fe-Mn alloys. These materials are used in diverse applications due to their different mechanical properties as well as the relatively low costs of the principal constituent elements (Fe, Mn). The Hadfield and the TWIP steels have most wide engineering usage whereas SMAs are being tentatively introduced into industrial settings; HEAs remain a promising research topic yet to be implemented in technological services. The common feature of these materials lies in their plastic deformation micromechanism particularly in the form of synergistic twinning and slipping. However, the predominance of either phenomenon differs from one class of alloy to another. Hadfield steels deform via concurrent slip and twinning, which is mechanistically similar for TWIP, however, with a relatively greater degree of twinning for the latter case. Consequently, both types of alloys are considered attractive candidates for high toughness applications, TWIP having an added advantage of higher strength-to-weight ratio. HEAs share similar mechanical attributes reportedly with more improved strength and ductility at low temperatures. Deformation-wise, they possess a unique characteristic of an enhanced twinning propensity, and hence superior toughness at cryogenic states. By contrast, the mechanical properties of Fe-Mn SMAs, deformation recoverability being their salient attribute, are primarily related with slip-assisted reversible crystal transformations.

By reviewing their mechanical responses and the underlying deformation mechanism, we have showcased the origin of their properties from the microstructural level. This could serve the materials and mechanics specialists with guidance for further improvement of engineering properties, say, by predisposing certain microscopic features to a greater or lesser extent. For instance, this could be achieved through regulating thermomechanical treatments, alloying etc. during the fabrication process. To that end, rapidly emerging physical models can also help reveal the required extent of alloying, rate dependence, thermodynamics etc., thereby facilitating the formulation of property improvement. With increasing computational power, simulations of defect evolution in a massive scale within the frameworks of crystal

plasticity, molecular dynamics etc. will decide the future of research in this regard. In this article, we have mostly discussed about uniaxial tensile/compressive properties, which constitute the fundamental understanding of mechanical attributes. Moreover, other outstanding engineering concerns remain such as achieving enhanced resistance to failures due to static fracture, fatigue, creep, thermomechanical fatigue etc., answers to which require continuous research both on experimental and theoretical grounds [290].

Acknowledgements

This study was sponsored by the Nyquist Chair funds and partially by NSF-CMMI 156288, which is gratefully acknowledged.

References

[1] Y. Lin, S. Wang, T. Chen, J. Mater. Process. Technol. 120 (2002) 126–132.
[2] B. Hutchinson, N. Ridley, Scr. Mater. 55 (2006) 299–302.
[3] B. De Cooman, O. Kwon, K. Chin, Mater. Sci. Technol. 28 (2012) 513–527.
[4] O. Grässel, L. Krüger, G. Frommeyer, L. Meyer, Int. J. Plast. 16 (2000) 1391–1409.
[5] D. Cornette, P. Cugy, A. Hildenbrand, M. Bouzekri, G. Lovato, Rev. Métall.–Int. J. Metall. 102 (2005) 905–918.
[6] T. Sawaguchi, T. Maruyama, H. Otsuka, A. Kushibe, Y. Inoue, K. Tsuzaki, Materi. Trans. 57 (2016) 283–293.
[7] B. Cantor, I. Chang, P. Knight, A. Vincent, Mater. Sci. Eng.: A 375 (2004) 213–218.
[8] B. Gludovatz, A. Hohenwarter, D. Catoor, E.H. Chang, E.P. George, R.O. Ritchie, Science 345 (2014) 1153–1158.
[9] J.W. Yeh, S.K. Chen, S.J. Lin, J.Y. Gan, T.S. Chin, T.T. Shun, C.H. Tsau, S.Y. Chang, Adv. Eng. Mater. 6 (2004) 299–303.
[10] R.A. Hadfield, Metallurgy and Its Influence on Modern Progress, JSTOR, 1925.
[11] K. Raghavan, A. Sastri, M. Marcinkowski, Trans. Metall. Soc. AIME 245 (1969) 1569–1575.
[12] W. Owen, M. Grujicic, Acta Mater. 47 (1998) 111–126.
[13] Y. Dastur, W. Leslie, Metall. Trans. A 12 (1981) 749–759.
[14] M. Shtremel, Phys. Metals Metallogr. (USSR) 63 (1987) 158–166.
[15] P. Adler, G. Olson, W. Owen, Metall. Mater. Trans. A 17 (1986) 1725–1737.
[16] C. Efstathiou, H. Sehitoglu, Acta Mater. 58 (2010) 1479–1488.
[17] C. Iglesias, G. Solórzano, B. Schulz, Mater. Charact. 60 (2009) 971–979.
[18] M. Abbasi, S. Kheirandish, Y. Kharrazi, J. Hejazi, Mater. Sci. Eng.: A 513 (2009) 72–76.
[19] E. Astafurova, Y.I. Chumlyakov, H. Maier, Int. J. Fract. 160 (2009) 143.
[20] D. Canadinc, H. Sehitoglu, H. Maier, Mater. Sci. Eng.: A 454 (2007) 662–666.
[21] E. Zakharova, I. Kireeva, Y.I. Chumlyakov, S. Efimenko, H. Sehitoglu, I. Karaman, Dokl. Phys. 47 (2002) 515–517 (Springer).
[22] I. Karaman, H. Sehitoglu, Y.I. Chumlyakov, H. Maier, I. Kireeva, Scr. Mater. 44 (2001) 337–343.
[23] I. Karaman, H. Sehitoglu, A. Beaudoin, Y. Chumlyakov, H. Maier, C. Tome, Acta Mater. 48 (2000) 2031–2047.
[24] I. Gutierrez-Urrutia, S. Zaefferer, D. Raabe, Mater. Sci. Eng.: A 527 (2010) 3552–3560.
[25] S. Allain, J.-P. Chateau, O. Bouaziz, Mater. Sci. Eng.: A 387 (2004) 143–147.
[26] S. Vercammen, B. Blanpain, B. De Cooman, P. Wollants, Acta Mater. 52 (2004) 2005–2012.
[27] R. Ueji, N. Tsuchida, D. Terada, N. Tsuji, Y. Tanaka, A. Takemura, K. Kunishige, Scr. Mater. 59 (2008) 963–966.
[28] O. Bouaziz, S. Allain, C. Scott, Scr. Mater. 58 (2008) 484–487.
[29] M. Shiekhelsouk, V. Favier, K. Inal, M. Cherkaoui, Int. J. Plast. 25 (2009) 105–133.
[30] T. Shun, C. Wan, J. Byrne, Acta Metall. Mater. 40 (1992) 3407–3412.
[31] Y.S. Chun, J. Lee, C.M. Bae, K.-T. Park, C.S. Lee, Scr. Mater. 67 (2012) 681–684.
[32] S. Curtze, V.-T. Kuokkala, Acta Mater. 58 (2010) 5129–5141.
[33] G. Frommeyer, U. Brüx, P. Neumann, ISIJ Int. 43 (2003) 438–446.
[34] A. Hamada, L. Karjalainen, Mater. Sci. Eng.: A 528 (2011) 1819–1827.
[35] A. Hamada, L. Karjalainen, J. Puustinen, Mater. Sci. Eng.: A 517 (2009) 68–77.
[36] H. Idrissi, K. Renard, L. Ryelandt, D. Schryvers, P. Jacques, Acta Mater. 58 (2010) 2464–2476.
[37] X.I.O.N.G. R.-g, F.U. R.-y, S. Yu, L. Qian, W.E.I. X.-c, L. Lin, J. Iron Steel Res. Int. 16 (2009) 8121–8186.
[38] S. Xu, D. Ruan, J.H. Beynon, Y. Rong, Mater. Sci. Eng.: A 573 (2013) 132–140.
[39] X. Wang, X. Sun, C. Song, H. Chen, W. Han, F. Pan, Mater. Sci. Eng.: A 698 (2017) 110–116.
[40] P. Chowdhury, H. Sehitoglu, Prog. Mater. Sci. 88 (2017) 49–88.
[41] A. Sato, T. Mori, Mater. Sci. Eng.: A 146 (1991) 197–204.
[42] A. Sato, E. Chishima, Y. Yamaji, T. Mori, Acta Metall. 32 (1984) 539–547.
[43] N. Bergeon, G. Guenin, C. Esnouf, Mater. Sci. Eng.: A 242 (1998) 77–86.
[44] N. Bergeon, G. Guenin, C. Esnouf, Mater. Sci. Eng.: A 242 (1998) 87–95.
[45] T. Omori, K. Ando, M. Okano, X. Xu, Y. Tanaka, I. Ohnuma, R. Kainuma, K. Ishida, Science 333 (2011) 68–71.
[46] L. Tseng, J. Ma, B. Hornbuckle, I. Karaman, G. Thompson, Z. Luo, Y. Chumlyakov, Acta Mater. 97 (2015) 234–244.
[47] L. Tseng, J. Ma, S. Wang, I. Karaman, Y. Chumlyakov, Scr. Mater. 116 (2016) 147–151.
[48] P. Chowdhury, H. Sehitoglu, Prog. Mater. Sci. 85 (2017) 1–42.
[49] A. Gali, E.P. George, Intermetallics 39 (2013) 74–78.
[50] M.C. Gao, D.E. Alman, Entropy 15 (2013) 4504–4519.
[51] C.-Y. Hsu, C.-C. Juan, S.-T. Chen, T.-S. Sheu, J.-W. Yeh, S.-K. Chen, JOM 65 (2013) 1829–1839.
[52] F. Otto, Y. Yang, H. Bei, E.P. George, Acta Mater. 61 (2013) 2628–2638.
[53] Z. Wu, H. Bei, G.M. Pharr, E.P. George, Acta Mater. 81 (2014) 428–441.
[54] J.-W. Yeh, S.-Y. Chang, Y.-D. Hong, S.-K. Chen, S.-J. Lin, Mater. Chem. Phys. 103 (2007) 41–46.
[55] Y. Zhang, X. Yang, P. Liaw, JOM 64 (2012) 830–838.
[56] Y. Zhou, Y. Zhang, Y. Wang, G. Chen, Appl. Phys. Lett. 90 (2007) 181904.
[57] X. Wang, Y. Zhang, Y. Qiao, G. Chen, Intermetallics 15 (2007) 357–362.
[58] S. Singh, N. Wanderka, B. Murty, U. Glatzel, J. Banhart, Acta Mater. 59 (2011) 182–190.
[59] C. Li, J. Li, M. Zhao, Q. Jiang, J. Alloys Compd. 475 (2009) 752–757.
[60] Y. Zhang, T.T. Zuo, Z. Tang, M.C. Gao, K.A. Dahmen, P.K. Liaw, Z.P. Lu, Prog. Mater. Sci. 61 (2014) 1–93.
[61] D. Subramanyam, A. Swansiger, H. Avery, Tenth Edition, ASM International, Metals Handbook, vol. 1(1990) , pp. 822–840.
[62] ASTM, Astm, (1940) .
[63] Y. Dastur, W. Leslie, Metall. Mater. Trans. A 12 (1981) 749–759.
[64] L. Remy, Acta Metall. 26 (1978) 443–451.
[65] E. Astafurova, V. Moskvina, G. Maier, E. Melnikov, G. Zakharov, S. Astafurov, H. Maier, Scr. Mater. 136 (2017) 101–105.
[66] I. Karaman, H. Sehitoglu, K. Gall, Y.I. Chumlyakov, H. Maier, Acta Mater. 48 (2000) 1345–1359.
[67] M. Byrnes, M. Grujicic, W. Owen, Acta Metall. 35 (1987) 1853–1862.
[68] J. Simmons, Mater. Sci. Eng.: A 207 (1996) 159–169.
[69] R.P. Reed, JOM J. Miner. Metals Mater. Soc. 41 (1989) 16–21.
[70] M. Speidel, High Nitrogen Steels–HNS 88 (1988) 92–96.
[71] F. Pickering, High Nitrogen Steels–HNS 88 (1988) 10–31.
[72] J. Raviers, G. Slavens, J. Mater. Eng. Perform. 4 (1995) 697–708.
[73] Y.I. Chumlyakov, I. Kireeva, A. Korotaev, E. Litvinova, Y.L. Zuev, Russ. Phys. J. 39 (1996) 189–210.
[74] Y.I. Chumlyakov, I. Kireeva, A. Korotaev, L. Aparova, Phys. Met. Metall. 75 (1993) 218–223.
[75] Y.I. Chumlyakov, I. Kireeva, H. Sehitoglu, E. Litvinova, E. Zaharova, N. Luzginova, Mater. Sci. Forum 318 (1999) 395–400 (Trans Tech Publ).
[76] D. Canadinc, H. Sehitoglu, I. Karaman, Y. Chumlyakov, H. Maier, Metall. Mater. Trans. A 34 (2003) 1821–1831.
[77] H. Berns, V. Gavriljuk, Springer-Verlag, Berlin Heidelberg, High nitrogen steels: structure, properties, manufacture, applications, (1999) .
[78] D. Canadinc, H. Sehitoglu, H. Maier, Y. Chumlyakov, Acta Mater. 53 (2005) 1831–1842.
[79] E.G. Astafurova, I.V. Kireeva, Y.I. Chumlyakov, H.J. Maier, H. Sehitoglu, Int. J. Mater. Res. 98 (2007) 144–149.
[80] B. Zuidema, D. Subramanyam, W. Leslie, Metall. Trans. A 18 (1987) 1629–1639.
[81] M. Abbasi, S. Kheirandish, Y. Kharrazi, J. Hejazi, Wear 268 (2010) 202–207.
[82] E. Astafurova, M. Tukeev, Y.I. Chumlyakov, Russ. Phys. J. 50 (2007) 959–963.
[83] D. Canadinc, C. Efstathiou, H. Sehitoglu, Scr. Mater. 59 (2008) 1103–1106.
[84] E. Bayraktar, F.A. Khalid, C. Levaillant, J. Mater. Process. Technol. 147 (2004) 145–154.
[85] M. Lindroos, M. Apostol, V. Heino, K. Valtonen, A. Laukkanen, K. Holmberg, V.-T. Kuokkala, Tribol. Lett. 57 (2015) 24.
[86] W. Wang, R. Song, S. Peng, Z. Pei, Mater. Des. 105 (2016) 96–105.
[87] I. Karaman, H. Sehitoglu, Y.I. Chumlyakov, H.J. Maier, I. Kireeva, Metall. Mater. Trans. A 32 (2001) 695–706.
[88] A.H. Cottrell, B. Bilby, Proc. Phys. Soc. London, Sect. A 62 (1949) 49.
[89] A. Cottrell, M. Jaswon, Proc. R. Soc. London A: Math. Phys. Eng. Sci. 199 (1949) 104–114 (The Royal Society).
[90] S. Van den Brink, A. Van Den Beukel, P. McCormick, Phys. Status Solidi (a) 30 (1975) 469–477.
[91] A. Van den Beukel, Phys. Status Solidi (a) 30 (1975) 197–206.
[92] N. Louat, Scr. Metall. 15 (1981) 1167–1170.
[93] P. McCormick, Acta Metall. 36 (1988) 3061–3067.
[94] Y. Estrin, P. McCormick, Acta Metall. Mater. 39 (1991) 2977–2983.
[95] P. McCormick, C. Ling, Acta Metall. Mater. 43 (1995) 1969–1977.
[96] J. Kang, D. Wilkinson, M. Jain, J. Embury, A. Beaudoin, S. Kim, R. Mishira, A. Sachdev, Acta Mater. 54 (2006) 209–218.
[97] J. Kang, D.S. Wilkinson, J.D. Embury, M. Jain, A.J. Beaudoin, Scr. Mater. 53 (2005) 499–503.
[98] H. Halim, D.S. Wilkinson, M. Niewczas, Acta Mater. 55 (2007) 4151–4160.
[99] D. Canadinc, H. Sehitoglu, H. Maier, D. Niklasch, Y. Chumlyakov, Int. J. Solids Struct. 44 (2007) 34–50.
[100] B. Bal, B. Gumus, D. Canadinc, J. Eng. Mater. Technol. 138 (2016) 031012.
[101] M.C. Uslu, D. Canadinc, J. Mater. Sci. 45 (2010) 1683–1687.
[102] B. Gumus, B. Bal, G. Gerstein, D. Canadinc, H. Maier, F. Guner, M. Elmadagli, Mater. Sci. Eng.: A 648 (2015) 104–112.
[103] M. Mirzajanzadeh, D. Canadinc, J. Eng. Mater. Technol. 138 (2016) 041004.
[104] O. Onal, C. Ozmenci, D. Canadinc, Front. Mater. 1 (2014) 16.
[105] F. Liu, B. Lv, F. Zhang, S. Yang, Mater. Lett. 65 (2011) 2333–2336.

[106] E. Astafurova, M. Tukeeva, G. Maier, E. Melnikov, H. Maier, Mater. Sci. Eng.: A 604 (2014) 166–175.
[107] K. Renard, S. Ryelandt, P. Jacques, Mater. Sci. Eng.: A 527 (2010) 2969–2977.
[108] H. Yang, Y. Tian, Z. Zhang, Z. Zhang, Mater. Sci. Eng.: A 655 (2016) 251–255.
[109] H. Yang, Z. Zhang, Y. Tian, Z. Zhang, Mater. Sci. Eng.: A 690 (2017) 146–157.
[110] S. Dancette, L. Delannay, K. Renard, M. Melchior, P. Jacques, Acta Mater. 60 (2012) 2135–2145.
[111] T. Niendorf, C. Rüsing, A. Frehn, Y. Chumlyakov, H. Maier, Scr. Mater. 67 (2012) 875–878.
[112] H.-G. Lambers, C. Rüsing, T. Niendorf, D. Geissler, J. Freudenberger, H. Maier, Int. J. Fatigue 40 (2012) 51–60.
[113] L. Zhang, X.-h. Liu, K.-y. Shu, J. Iron Steel Res. Int. 18 (2011) 4548–4564.
[114] B. Bal, B. Gumus, G. Gerstein, D. Canadinc, H. Maier, Mater. Sci. Eng.: A 632 (2015) 29–34.
[115] B. Gumus, B. Bal, G. Gerstein, D. Canadinc, H. Maier, Mater. Sci. Technol. 32 (2016) 463–465.
[116] F. Otto, A. Dlouhý, C. Somsen, H. Bei, G. Eggeler, E.P. George, Acta Mater. 61 (2013) 5743–5755.
[117] F. Ayari, T. Lazghab, E. Bayraktar, Comput. Mater. Sci. Surf. Eng. (2009) 1–2.
[118] Y. Wei, Y. Li, L. Zhu, Y. Liu, X. Lei, G. Wang, Y. Wu, Z. Mi, J. Liu, H. Wang, Nat. Commun. 5 (2014).
[119] S. Kibey, J. Liu, M. Curtis, D. Johnson, H. Sehitoglu, Acta Mater. 54 (2006) 2991–3001.
[120] N. Kulikov, C. Demangeat, Phys. Rev. B 55 (1997) 3533.
[121] M.B. Stearns, Phys. Rev. 147 (1966) 439.
[122] J.-A. Yan, C.-Y. Wang, S.-Y. Wang, Phys. Rev. B 70 (2004) 174105.
[123] S. Allain, J.-P. Chateau, O. Bouaziz, S. Migot, N. Guelton, Mater. Sci. Eng.: A 387 (2004) 158–162.
[124] J.W. Christian, S. Mahajan, Prog. Mater. Sci. 39 (1995) 1–157.
[125] B. Decelis, A.S. Argon, S. Yip, J. Appl. Phys. 54 (1983) 4864–4878.
[126] C. Domain, G. Monnet, Phys. Rev. Lett. 95 (2005) 215506.
[127] G. Sainath, B. Choudhary, T. Jayakumar, Comput. Mater. Sci 104 (2015) 76–83.
[128] M. Easton, W.Q. Song, T. Abbott, Mater. Des. 27 (2006) 935–946.
[129] L.C. Campanelli, U.F.H. Suhuddin, A.Í.S. Antonialli, J.F. dos Santos, N.G. de Alcantara, C. Bolfarini, J. Mater. Process. Technol. 213 (2013) 515–521.
[130] J. Yan, Z. Xu, Z. Li, L. Li, S. Yang, Scr. Mater. 53 (2005) 585–589.
[131] T. Hilditch, D. Atwell, M. Easton, M. Barnett, Mater. Des. 30 (2009) 2316–2322.
[132] J. Hirsch, T. Al-Samman, Acta Mater. 61 (2013) 818–843.
[133] M. Naderi, V. Uthaisangsuk, U. Prahl, W. Bleck, Steel Res. Int. 79 (2008) 77–84.
[134] W. Bleck, S. Papaefthymiou, A. Frehn, Steel Res. Int. 75 (2004) 704–710.
[135] U. Diekmann, T. Säuberlich, A. Frehn, ATZ-Automobiltech. Z. 109 (2007) 1128–1135.
[136] H.-H. Bok, M.-G. Lee, E.J. Pavlina, F. Barlat, H.-D. Kim, Int. J. Mech. Sci. 53 (2011) 744–752.
[137] C.P. Kohar, M. Cherkaoui, H. El Kadiri, K. Inal, Int. J. Plast. 84 (2016) 224–254.
[138] K. Omer, L. ten Kortenaar, C. Butcher, M. Worswick, S. Malcolm, D. Detwiler, Int. J. Impact Eng. 103 (2017) 12–28.
[139] A. Dumay, J.-P. Chateau, S. Allain, S. Migot, O. Bouaziz, Mater. Sci. Eng.: A 483 (2008) 184–187.
[140] B. Huang, X. Wang, Y. Rong, L. Wang, L. Jin, Mater. Sci. Eng.: A 438 (2006) 306–311.
[141] B. Huang, X. Wang, L. Wang, Y. Rong, Metall. Mater. Trans. A 39 (2008) 717–724.
[142] J. Zrnik, O. Muransky, O. Stejskal, P. Lukáš, P. Hornak, Mater. Sci. Eng.: A 483 (2008) 71–75.
[143] L. Robertson, T. Hilditch, P. Hodgson, Int. J. Fatigue 30 (2008) 587–594.
[144] T. Iwamoto, T. Tsuta, Int. J. Plast. 16 (2000) 791–804.
[145] P. Jacques, Q. Furnémont, F. Lani, T. Pardoen, F. Delannay, Acta Mater. 55 (2007) 3681–3693.
[146] Y. Wen, H. Peng, H. Si, R. Xiong, D. Raabe, Mater. Des. 55 (2014) 798–804.
[147] J. Jeong, W. Woo, K. Oh, S. Kwon, Y. Koo, Acta Mater. 60 (2012) 2290–2299.
[148] X. Feng, F. Zhang, Z. Yang, M. Zhang, Wear 305 (2013) 299–304.
[149] M.M. Atabaki, S. Jafari, H. Abdollah-pour, J. Iron Steel Res. Int. 19 (2012) 43–50.
[150] J. Kang, F. Zhang, X. Long, B. Lv, Mater. Sci. Eng.: A 591 (2014) 59–68.
[151] Y.N. Petrov, V.G. Gavriljuk, H. Berns, F. Schmalt, Wear 260 (2006) 687–691.
[152] C. Efstathiou, H. Sehitoglu, Mater. Sci. Eng.: A 506 (2009) 174–179.
[153] S. Kibey, J. Liu, D. Johnson, H. Sehitoglu, Acta Mater. 55 (2007) 6843–6851.
[154] J.G. Lee, C. Lim, H. Kim, S. Hong, M. Kim, B. Kang, D. Park, M. Lee, C. Rhee, Powder Technol. 228 (2012) 254–257.
[155] H.-W. Yen, M. Huang, C. Scott, J.-R. Yang, Scr. Mater. 66 (2012) 1018–1023.
[156] K. Jeong, J.-E. Jin, Y.-S. Jung, S. Kang, Y.-K. Lee, Acta Mater. 61 (2013) 3399–3410.
[157] S.-J. Lee, J. Kim, S.N. Kane, B.C. De Cooman, Acta Mater. 59 (2011) 6809–6819.
[158] L. Mosecker, D. Pierce, A. Schwedt, M. Beighmohamadi, J. Mayer, W. Bleck, J. Wittig, Mater. Sci. Eng.: A 642 (2015) 71–83.
[159] L. Chen, H.-S. Kim, S.-K. Kim, B. De Cooman, ISIJ Int. 47 (2007) 1804–1812.
[160] W. Song, T. Ingendahl, W. Bleck, Acta Metall. Sin. (Engl. Lett.) 27 (2014) 546–556.
[161] K. Renard, P. Jacques, Mater. Sci. Eng.: A 542 (2012) 8–14.
[162] S. Allain, J.-P. Chateau, D. Dahmoun, O. Bouaziz, Mater. Sci. Eng.: A 387 (2004) 272–276.
[163] J.-E. Jin, Y.-K. Lee, Acta Mater. 60 (2012) 1680–1688.
[164] S.-h. Wang, Z.-y. Liu, G.-d. Wang, J.-L. Liu, G.-F. Liang, Q.-L. Li, J. Iron Steel Res. Int. 17 (2010) 70–74.
[165] N. Li, Y. Wang, R.L. Peng, X. Sun, P.K. Liaw, G. Wu, L. Wang, H. Cai, Acta Mater. 59 (2011) 6369–6377.
[166] A. Khosravifard, A. Hamada, M. Moshksar, R. Ebrahimi, D. Porter, L. Karjalainen, Mater. Sci. Eng.: A 582 (2013) 15–21.
[167] D. Geissler, J. Freudenberger, A. Kauffmann, M. Krautz, H. Klauss, A. Voss, J. Eickemeyer, L. Schultz, Acta Mater. 59 (2011) 7711–7723.
[168] T. Niendorf, C. Lotze, D. Canadinc, A. Frehn, H. Maier, Mater. Sci. Eng.: A 499 (2009) 518–524.
[169] A. Glage, C. Weigelt, J. Räthel, H. Biermann, Int. J. Fatigue 65 (2014) 9–17.
[170] Y.W. Kim, G. Kim, S.-G. Hong, C.S. Lee, Mater. Sci. Eng.: A 528 (2011) 4696–4702.
[171] A. Hamada, L. Karjalainen, Mater. Sci. Eng.: A 527 (2010) 5715–5722.
[172] I. Nikulin, T. Sawaguchi, K. Tsuzaki, Mater. Sci. Eng.: A 587 (2013) 192–200.
[173] A. Hamada, L. Karjalainen, M. Somani, Mater. Sci. Eng.: A 467 (2007) 114–124.
[174] F. Reyes-Calderón, I. Mejía, A. Boulaajaj, J. Cabrera, Mater. Sci. Eng.: A 560 (2013) 552–560.
[175] K.-G. Chin, C.-Y. Kang, S.Y. Shin, S. Hong, S. Lee, H.S. Kim, K.-h. Kim, N.J. Kim, Mater. Sci. Eng.: A 528 (2011) 2922–2928.
[176] S. Hong, J. Lee, B.-J. Lee, H.S. Kim, S.-K. Kim, K.-G. Chin, S. Lee, Mater. Sci. Eng.: A 587 (2013) 85–99.
[177] S. Toker, D. Canadinc, A. Taube, G. Gerstein, H. Maier, Mater. Sci. Eng.: A 593 (2014) 120–126.
[178] C. Sun, N. Guo, M. Fu, S. Wang, Int. J. Plast. 76 (2016) 186–212.
[179] B. De Cooman, J. Kim, S. Lee, Scr. Mater. 66 (2012) 986–991.
[180] K. Yan, D.G. Carr, M.D. Callaghan, K.-D. Liss, H. Li, Scr. Mater. 62 (2010) 246–249.
[181] C. Haase, O. Kremer, W. Hu, T. Ingendahl, R. Lapovok, D.A. Molodov, Acta Mater. 107 (2016) 239–253.
[182] D.R. Steinmetz, T. Jäpel, B. Wietbrock, P. Eisenlohr, I. Gutierrez-Urrutia, A. Saeed-Akbari, T. Hickel, F. Roters, D. Raabe, Acta Mater. 61 (2013) 494–510.
[183] A. Prakash, T. Hochrainer, E. Reisacher, H. Riedel, Steel Res. Int. 79 (2008) 645–652.
[184] A.A. Saleh, E.V. Pereloma, A.A. Gazder, Acta Mater. 61 (2013) 2671–2691.
[185] R. Quey, P. Dawson, F. Barbe, Comput. Methods Appl. Mech. Eng. 200 (2011) 1729–1745.
[186] F. Roters, P. Eisenlohr, L. Hantcherli, D.D. Tjahjanto, T.R. Bieler, D. Raabe, Acta Mater. 58 (2010) 1152–1211.
[187] F. Barbe, L. Decker, D. Jeulin, G. Cailletaud, Int. J. Plast. 17 (2001) 513–536.
[188] P. Van Houtte, S. Li, M. Seefeldt, L. Delannay, Int. J. Plast. 21 (2005) 589–624.
[189] R.A. Lebensohn, C. Tomé, Acta Metall. Mater. 41 (1993) 2611–2624.
[190] R.A. Lebensohn, C. Tomé, Mater. Sci. Eng.: A 175 (1994) 71–82.
[191] C. Tomé, R.A. Lebensohn, U. Kocks, Acta Metall. Mater. 39 (1991) 2667–2680.
[192] S.R. Kalidindi, Int. J. Plast. 17 (2001) 837–860.
[193] S.R. Kalidindi, J. Mech. Phys. Solids 46 (1998) 267273–271290.
[194] C. Ozmenci, MS, Thesis, Koc University, Istanbul, 2015.
[195] M. Koyama, Z. Zhang, M. Wang, D. Ponge, D. Raabe, K. Tsuzaki, H. Noguchi, C.C. Tasan, Science 355 (2017) 1055–1057.
[196] G. Monnet, D. Terentyev, Acta Mater. 57 (2009) 1416–1426.
[197] L. Proville, D. Rodney, M.-C. Marinica, Nat. Mater. 11 (2012) 845.
[198] P. Gordon, T. Neeraj, Y. Li, J. Li, Modell. Simul. Mater. Sci. Eng. 18 (2010) 085008.
[199] N.N. Kumar, R. Tewari, P. Durgaprasad, B. Dutta, G. Dey, Comput. Mater. Sci 77 (2013) 260–263.
[200] D. Li, H. Zbib, X. Sun, M. Khaleel, Int. J. Plast. 52 (2014) 3–17.
[201] G.B. Olson, Science 288 (2000) 993–998.
[202] P.B. Chowdhury, Modeling Mechanical Properties–linking Atomistics to Continuum, University of Illinois at Urbana-Champaign, 2016.
[203] P. Chowdhury, L. Patriarca, G. Ren, H. Sehitoglu, Int. J. Plast. 81 (2016) 152–167.
[204] P. Chowdhury, G. Ren, H. Sehitoglu, Philos. Mag. Lett. 95 (2015) 574–586.
[205] H. Sehitoglu, I. Karaman, X.Y. Zhang, Y. Chumlyakov, H.J. Maier, Scr. Mater. 44 (2001) 779–784.
[206] H. Sehitoglu, X.Y. Zhang, T. Kotil, D. Canadinc, Y. Chumlyakov, H.J. Maier, Metall. Mater. Trans. A: Phys. Metall. Mater. Sci. 33 (2002) 3661–3672.
[207] T. Maki, K. Kobayashi, M. Minato, I. Tamura, Scr. Metall. 18 (1984) 1105–1109.
[208] T. Sohmura, R. Oshima, F.E. Fujita, Scr. Metall. 14 (1980) 855–856.
[209] F. Xiao, T. Fukuda, T. Kakeshita, Philos. Mag. 95 (2015) 1390–1398.
[210] Y. Tanaka, Y. Himuro, R. Kainuma, Y. Sutou, T. Omori, K. Ishida, Science 327 (2010) 1488–1490.
[211] N. Jost, Mater. Sci. Eng.: A 273–275 (1999) 649–653.
[212] Y.N. Koval, V.V. Kokorin, L.G. Khandros, Phys. Met. Metallogr. 48 (1979) 162–164.
[213] K. Otsuka, C.M. Wayman, Shape Memory Materials, Cambridge University Press, 1999.
[214] A. Sato, E. Chishima, K. Soma, T. Mori, Acta Metall. 30 (1982) 1177–1183.
[215] Y.H. Wen, H.B. Peng, D. Raabe, I. Gutierrez-Urrutia, J. Chen, Y.Y. Du, Nat. Commun. 5 (2014).
[216] P. Krooc, C. Somsen, T. Niendorf, M. Schaper, I. Karaman, Y. Chumlyakov, G. Eggeler, H.J. Maier, Acta Mater. 79 (2014) 126–137.
[217] M. Vollmer, C. Segel, P. Krooß, J. Günther, L.W. Tseng, I. Karaman, A. Weidner, H. Biermann, T. Niendorf, Scr. Mater. 108 (2015) 23–26.
[218] M. Vollmer, P. Krooß, M.J. Kriegel, V. Klemm, C. Somsen, H. Ozcan, I. Karaman, A. Weidner, D. Rafaja, H. Biermann, T. Niendorf, Scr. Mater. 114 (2016) 156–160.
[219] T. Niendorf, F. Brenne, P. Krooc, M. Vollmer, J. Gunther, D. Schwarze, H. Biermann, Metall. Mater. Trans. A: Phys. Metall. Mater. Sci. 47 (2016) 2569–2573.
[220] S. Cotes, M. Sade, A.F. Guillermet, Metall. Mater. Trans. A 26 (1995) 1957–1969.

[221] A. Sato, E. Chishima, K. Soma, T. Mori, Acta Metall. 30 (1982) 1177–1183.
[222] A. Sato, H. Kubo, T. Maruyama, Materi. Trans. 47 (2006) 571–579.
[223] Y. Wen, H. Peng, D. Raabe, I. Gutiérrez-Urrutia, J. Chen, Y. Du, Nat. Commun. 5 (2014).
[224] N. Bergeon, G. Guenin, C. Esnouf, Mater. Sci. Eng.: A 238 (1997) 309–316.
[225] J. Yang, C. Wayman, Metall. Trans. A 23 (1992) 1445–1454.
[226] A. Sato, T. Mori, Mater. Sci. Eng.: A 146 (1991) 197–204.
[227] A. Druker, V. Fuster, L. Isola, R. Bolmaro, J. Malarría, Procedia Mater. Sci. 9 (2015) 187–194.
[228] S. Kajiwara, Mater. Sci. Eng.: A 273 (1999) 67–88.
[229] D. Liu, S. Kajiwara, T. Kikuchi, N. Shinya, Philos. Mag. 83 (2003) 2875–2897.
[230] D. Liu, S. Kajiwara, T. Kikuchi, N. Shinya, D. Wang, W. Liu, Mater. Trans. JIM 41 (2000) 593–596.
[231] Q. Gu, J. Van Humbeeck, L. Delaey, J. Phys. IV 4 (1994) (C3-135-C133-144).
[232] H. Otsuka, H. Yamada, T. Maruyama, H. Tanahashi, S. Matsuda, M. Murakami, ISIJ Int. 30 (1990) 674–679.
[233] N.E. Stanford, K. Chen, D.P. Dunne, X.-J. Jin, ISIJ Int. 47 (2007) 883–889.
[234] N. Stanford, D.P. Dunne, H. Li, Scr. Mater. 58 (2008) 583–586.
[235] L. Remy, A. Pineau, Mater. Sci. Eng. 28 (1977) 99–107.
[236] J.P. Hirth, J. Lothe, Theory of dislocations, (1982) .
[237] E.B. Tadmor, R.E. Miller, Modeling Materials: Continuum, Atomistic and Multiscale Techniques, Cambridge University Press, 2011.
[238] W.A. Curtin, R.E. Miller, Modell. Simul. Mater. Sci. Eng. 11 (2003) R33.
[239] L. Tseng, J. Ma, S. Wang, I. Karaman, M. Kaya, Z. Luo, Y. Chumlyakov, Acta Mater. 89 (2015) 374–383.
[240] H. Sehitoglu, I. Karaman, R. Anderson, X. Zhang, K. Gall, H. Maier, Y. Chumlyakov, Acta Mater. 48 (2000) 3311–3326.
[241] W. Burgers, Physica 1 (1934) 561–586.
[242] A. Bogers, W. Burgers, Acta Metall. 12 (1964) 255–261.
[243] G. Olson, M. Cohen, Metall. Trans. A 7 (1976) 1897–1904.
[244] G. Olson, M. Cohen, Metall. Trans. A 7 (1976) 1905–1914.
[245] J.-W. Yeh, S.-J. Lin, T.-S. Chin, J.-Y. Gan, S.-K. Chen, T.-T. Shun, C.-H. Tsau, S.-Y. Chou, Metall. Mater. Trans. A 35 (2004) 2533–2536.
[246] Y. Zhang, G. Chen, C. Gan, J. ASTM Int. 7 (2010) 1–8.
[247] A. Zaddach, C. Niu, C. Koch, D. Irving, Jom 65 (2013) 1780–1789.
[248] P. Chowdhury, H. Sehitoglu, W. Abuzaid, H. Maier, Int. J. Plast. 71 (2015) 32–61.
[249] Y. Gong, C. Wen, Y. Li, X. Wu, L. Cheng, X. Han, X. Zhu, Mater. Sci. Eng.: A 569 (2013) 144–149.
[250] H. Bahmanpour, A. Kauffmann, M. Khoshkhoo, K. Youssef, S. Mula, J. Freudenberger, J. Eckert, R. Scattergood, C. Koch, Mater. Sci. Eng.: A 529 (2011) 230–236.
[251] P.-L. Sun, Y. Zhao, J. Cooley, M. Kassner, Z. Horita, T. Langdon, E. Lavernia, Y. Zhu, Mater. Sci. Eng.: A 525 (2009) 83–86.
[252] S. Huang, W. Li, S. Lu, F. Tian, J. Shen, E. Holmström, L. Vitos, Scr. Mater. 108 (2015) 44–47.
[253] M.F. Ashby, K. Johnson, Materials and Design: The Art and Science of Material Selection in Product Design, Butterworth-Heinemann, 2013.
[254] R.O. Ritchie, Nat. Mater. 10 (2011) 817–822.
[255] G. Laplanche, A. Kostka, O. Horst, G. Eggeler, E. George, Acta Mater. 118 (2016) 152–163.
[256] Z. Wu, C. Parish, H. Bei, J. Alloys Compd. 647 (2015) 815–822.
[257] S.P. Baker, Mater. Sci. Eng.: A 319 (2001) 16–23.
[258] R.J. Asaro, S. Suresh, Acta Mater. 53 (2005) 3369–3382.
[259] E. Hall, Proc. Phys. Soc. London, Sect. B 64 (1951) 747.
[260] N. Petch, J. Iron Steel Inst. 174 (1953) 25–28.
[261] L. Lu, Y. Shen, X. Chen, L. Qian, K. Lu, Science 304 (2004) 422–426.
[262] C. Deng, F. Sansoz, Acta Mater. 57 (2009) 6090–6101.
[263] J. Kacher, B. Eftink, B. Cui, I. Robertson, Curr. Opin. Solid State Mater. Sci. 18 (2014) 227–243.
[264] T. Zhu, H. Gao, Scr. Mater. 66 (2012) 843–848.
[265] P. Chowdhury, H. Sehitoglu, H. Maier, R. Rateick, Int. J. Plast. 79 (2016) 237–258.
[266] E.K. Gross, R.M. Dreizler, Density Functional Theory, Springer Science & Business Media, 2013.
[267] M. Parrinello, A. Rahman, J. Appl. Phys. 52 (1981) 7182–7190.
[268] W. Mills, Int. Mater. Rev. 42 (1997) 45–82.
[269] L. Lu, X. Chen, X. Huang, K. Lu, Science 323 (2009) 607–610.
[270] K. Lu, L. Lu, S. Suresh, Science 324 (2009) 349–352.
[271] P.B. Chowdhury, H. Sehitoglu, R.G. Rateick, H.J. Maier, Acta Mater. 61 (2013) 2531–2547.
[272] P. Chowdhury, H. Sehitoglu, R. Rateick, Curr. Opin. Solid State Mater. Sci. 20 (2016) 140–150.
[273] P. Chowdhury, Fatigue Crack Growth (FCG) Modeling in the Presence of Nano-Obstacles, (2012) .
[274] S. Alkan, P. Chowdhury, H. Sehitoglu, R.G. Rateick, H.J. Maier, Int. J. Fatigue 84 (2016) 28–39.
[275] P.B. Chowdhury, H. Sehitoglu, R.G. Rateick, Int. J. Fatigue 68 (2014) 277–291.
[276] P.B. Chowdhury, H. Sehitoglu, R.G. Rateick, Int. J. Fatigue 68 (2014) 292–301.
[277] P. Chowdhury, H. Sehitoglu, Fatigue Fract. Eng. Mater. Struct. 39 (2016) 652–674.
[278] P. Villars, H. Okamoto, K. Cenzual, ASM alloy phase diagrams database, ASM International, Materials Park, OH, USA, 2006.
[279] C.-J. Tong, Y.-L. Chen, J.-W. Yeh, S.-J. Lin, S.-K. Chen, T.-T. Shun, C.-H. Tsau, S.-Y. Chang, Metall. Mater. Trans. A 36 (2005) 881–893.
[280] C. Zhang, F. Zhang, S. Chen, W. Cao, Jom 64 (2012) 839–845.
[281] O.N. Senkov, F. Zhang, J.D. Miller, Entropy 15 (2013) 3796–3809.
[282] F. Zhang, C. Zhang, S. Chen, J. Zhu, W. Cao, U. Kattner, Calphad 45 (2014) 1–10.
[283] J. Kubler, K.-H. Hock, J. Sticht, A. Williams, J. Phys. F: Met. Phys. 18 (1988) 469.
[284] Y.-M. Kim, Y.-H. Shin, B.-J. Lee, Acta Mater. 57 (2009) 474–482.
[285] T. Gebhardt, D. Music, M. Ekholm, I. Abrikosov, J. Von Appen, R. Dronskowski, D. Wagner, J. Mayer, J. Schneider, Acta Mater. 59 (2011) 1493–1501.
[286] T. Gebhardt, D. Music, D. Kossmann, M. Ekholm, I.A. Abrikosov, L. Vitos, J.M. Schneider, Acta Mater. 59 (2011) 3145–3155.
[287] S. Reeh, D. Music, T. Gebhardt, M. Kasprzak, T. Jäpel, S. Zaefferer, D. Raabe, S. Richter, A. Schwedt, J. Mayer, Acta Mater. 60 (2012) 6025–6032.
[288] P. Chowdhury, H. Sehitoglu, Scr. Mater. 119 (2016) 82–87.
[289] V. Vitek, Philos. Mag. 18 (1968) 773–786.
[290] C. Chen, B. Lv, F. Wang, F. Zhang, Mater. Sci. Eng.: A 695 (2017) 144–153.